

Seasonal Flows on Warm Martian Slopes

Alfred S. McEwen,^{1*} Lujendra Ojha,¹ Colin M. Dundas,² Sarah S. Mattson,¹ Shane Byrne,¹ James J. Wray,³ Selby C. Cull,⁴ Scott L. Murchie,⁵ Nicolas Thomas,⁶ Virginia C. Gulick⁷

Water probably flowed across ancient Mars, but whether it ever exists as a liquid on the surface today remains debatable. Recurring slope lineae (RSL) are narrow (0.5 to 5 meters), relatively dark markings on steep (25° to 40°) slopes; repeat images from the Mars Reconnaissance Orbiter High Resolution Imaging Science Experiment show them to appear and incrementally grow during warm seasons and fade in cold seasons. They extend downslope from bedrock outcrops, often associated with small channels, and hundreds of them form in some rare locations. RSL appear and lengthen in the late southern spring and summer from 48°S to 32°S latitudes favoring equator-facing slopes, which are times and places with peak surface temperatures from ~250 to 300 kelvin. Liquid brines near the surface might explain this activity, but the exact mechanism and source of water are not understood.

Although there is much morphological evidence for water flow on Mars in the past, little definitive evidence exists for surface water today. The chloride and sulfate minerals on Mars are indicative of widespread and abundant brines in Mars geologic history (1–5). Salts can depress the freezing point of water by up to 70 K and reduce the evaporation rate by factors of 10 or more, so brines would be far more stable than pure water at the surface of Mars (2, 6–10). Here we describe observations by the High Resolution Imaging Science Experiment (HiRISE) (11) on the Mars Reconnaissance Orbiter (MRO) of features we call recurring slope lineae (RSL). RSL are narrow (0.5- to 5-m) markings, up to ~40% darker than their surroundings, on steep slopes (>25°; table S2); and they are recurring, forming and growing in warm seasons (late spring to early fall) and fading or vanishing in cold seasons. Confirmed RSL have been found to date at seven locations (Table 1), often with many separate clusters. There are 12 other likely RSL sites and 20 candidate sites. They extend downslope from bedrock outcrops or rocky areas and are often associated with small channels (Figs. 1 and 2 and figs. S3 to S5). RSL have lengths up to hundreds of meters, and more than 10³ lineae may be present in a HiRISE observation. Along with several other hypotheses, we explore the potential of briny flows as a formation mechanism of RSL.

Our survey of HiRISE images of steep slopes [supporting online material (SOM)] has identified confirmed and likely RSL only in the southern hemisphere from 32°S to 48°S, favoring equator-facing slopes (table S1). There are also eight candidate RSL sites in equatorial re-

gions (18°S to 19°N), but they are few in number at each site, and the seasonal recurrence has not been confirmed (table S3 and fig. S6). Where repeat imaging within a Mars year is available, RSL are observed to form and grow from late southern spring to early fall, and to fade or disappear in other seasons [L_S (the areocentric longitude of the Sun) = 20 to 245] (12) (figs. S1 and S2). RSL extend down the topographic gradient, diverting around obstacles rather than overtopping them. Individual lineae may split or merge. Because they terminate on steep slopes, RSL lengths must be controlled by a limited volume of mobile material.

There are up to five images per season for confirmed RSL sites, which show that they grow incrementally but not concurrently at uniform rates (SOM) (13). Some RSL may be unchanged between images (typically a few weeks or months apart in time), whereas others have lengthened by small or substantial amounts. Measured growth rates range from 0 to 20 m/day on average (fig. S3), but given sparse temporal coverage it could be as much as 560 m per event, with no other activity over several weeks.

RSL occur in the classical dark regions of Mars, which have moderate thermal inertias (~200 to 340 J m⁻² s^{-1/2} K⁻¹) (table S3); the bed-

rock outcrops probably have much higher thermal inertias. Determining the composition of RSL from orbit is challenging, as they are much smaller than the ~18 m-per-pixel scale of MRO's Compact Reconnaissance Imaging Spectrometer for Mars (CRISM) (14). RSL cover a substantial fraction of resolvable slopes in some areas (Figs. 1 and 2), but no distinctive spectral features have been identified, including the strong absorption features expected from even small quantities of water. Hydrated minerals are associated with bedrock at several RSL sites, such as phyllosilicates in Asimov Crater and chlorite, kaolinite, and hydrated silica in the central structure of Horowitz Crater (15), but there is no known correlation between RSL regions and particular minerals (SOM).

Slopes containing RSL are steep, near the angle of repose for cohesionless particles (table S2), and appear to be sites of active mass wasting (no superimposed aeolian bedforms). Numerous small channels (1 to 50 m wide) often cover these slopes, but RSL are rarely associated with the larger Martian gullies (ravines). RSL are found in only ~1% as many HiRISE images as are gullies. In a few cases (Fig. 1 and figs. S3 to S5), the presence and lengths of RSL are so similar to those of the fine channels that a genetic association seems likely, although cause and effect are not clear. Topographic changes associated with RSL have not been observed.

Other Martian slope features may appear similar to RSL. The seasonal, latitudinal, and slope aspect distribution of RSL and their occurrence in regions with a low dust index distinguish them from slope streaks (16) (Table 2). Small slope lineaments are also seen on high-latitude dunes and in a few non-dune gully alcoves during late winter and spring, as the seasonal CO₂ cover is sublimating. Although it has been proposed that the dune streaks are due to brines (17), the alternate hypothesis of sand flows initiated by CO₂ sublimation has been confirmed by the appearance of new dune gullies (18). Other dry mass-wasting features may resemble RSL, but lack seasonal recurrence.

Table 1. RSL types.

RSL type	Description and seasonal behaviors	Number of sites	Latitude range	Number of RSL per site
Confirmed RSL	Observed to recur in multiple warm seasons and fade in cold seasons	7	48°S to 32°S	10 ² to 10 ³
Likely RSL	Evidence for fading in cold seasons, but not yet observed to recur in multiple years	12	47°S to 34°S	10 to 10 ³
Candidate equatorial RSL	Morphology and geologic setting of RSL, changes observed, but seasonality unclear	8	18°S to 19°N	10 to 10 ²
Candidate RSL poleward of 30°S	Morphology and geologic setting of RSL, but no repeat imaging	12	52°S to 31°S	10 to 10 ³

¹Lunar and Planetary Laboratory, University of Arizona, Tucson, AZ 85721, USA. ²U.S. Geological Survey, Flagstaff, AZ 86001, USA. ³Department of Astronomy, Cornell University, Ithaca, NY 14853, USA. ⁴Department of Earth and Planetary Sciences, Washington University, St. Louis, MO 63130, USA. ⁵Johns Hopkins University Applied Physics Laboratory, Laurel, MD 20723, USA. ⁶Physikalisches Institut, University of Bern, Bern, Switzerland. ⁷NASA Ames Research Center and SETI Institute, Moffett Field, CA 94035, USA.

*To whom correspondence should be addressed. E-mail: mcewen@lpl.arizona.edu

The seasonal, latitudinal, and slope aspect distributions show that RSL require relatively warm temperatures. Summertime afternoon brightness temperatures measured from orbit (19) on RSL-covered slopes in the middle to late afternoon range from 250 to 300 K, with daily peak temperatures probably being higher (table S1). Equatorial regions reach temperatures comparable to warm-season temperatures on equator-facing slopes in the southern mid-latitudes. Northern summers are cooler because perihelion occurs shortly before the northern winter solstice. In spite of the equatorial candidates, RSL are clearly most abundant in the southern mid-latitudes.

A range of hypotheses must be considered to explain these observations. Thermal cycling can damage rocks (20) and might eventually trigger rock falls and dry granular flows, but is a very slow process. Another hypothesis is that adsorbed

water, which makes grains sticky, is released at high temperatures, allowing dry mass wasting, but the association with bedrock and rocky slopes is left unexplained. Triggering by seasonally high winds or dust devils is possible, but doesn't explain the absence of RSL in the northern hemisphere or the orientation preference of the mid-latitude features. None of these hypotheses explain why RSL are abundant in rare places and absent from most steep rocky slopes; other difficulties are listed in table S5. Nevertheless, all of these hypotheses deserve further consideration.

The latitudinal preference of RSL and their fading in cold seasons suggest some role for a volatile. CO₂ sublimation drives many dynamic phenomena on Mars (18), but CO₂ probably never freezes on these equator-facing slopes and certainly is not present in the summer. Nearly pure H₂O, if present, might drive activity, but (i)

the ice would rapidly sublimate to dry out these warm slopes, and (ii) some RSL activity occurs below the freezing point for pure water (table S1).

The definite association between RSL and temperatures greater than 250 K points to brines as the most relevant volatile. The Spirit landing site in Gusev Crater (14.6°S) reaches temperatures similar to those of the RSL slopes (table S1); the subsurface temperature at the hottest times should exceed 250 K down to at least 2 cm depth (21). Many brines expected on Mars have eutectic temperatures (T_e) below 250 K, except most sulfates (2, 10); RSL have not been found near the extensive sulfate deposits mapped from orbit (4). The most likely brine compositions relevant to RSL are chlorides (Mg, Na, or Ca) or Fe sulfates, with T_e from 205 to 250 K.

Brines could lead to RSL from seeps or thin flows. The formation mechanism could resemble that of (22) for putative "wet" slope streaks, in which the warm-season temperature exceeds T_e at depths of a few centimeters, brines percolate and refreeze at depth to form an impermeable layer, and downslope percolation occurs at the interface between liquid and frozen brine. Alternatively, a thin debris flow might be mobilized at the liquid/ice interface. This model should be more effective over surfaces with moderate to high thermal inertias, warming a thicker layer above the brine eutectic. For either seeping or debris flow, sufficient water to fill pore spaces is needed; interfacial water (23) is probably not sufficient. Given the lack of water absorption bands in CRISM spectra, we assume that RSL are usually dry at the surface, perhaps wet only in the subsurface and perhaps in small surface areas while moving.

The origin of the water to form RSL could be the absorption of water vapor by hygroscopic salts (deliquescence) or subsurface seeps. Deliquescence from the atmosphere, most likely in the polar regions where relative humidity is higher, might occur in the middle latitudes (10), although it is unclear whether sufficient water can be trapped each year. Deliquescence might also result from sublimation of relict subsurface ice and the diffusion of water vapor toward the surface (SOM). RSL formation would be localized by concentrations of hygroscopic salts and water vapor, in addition to other factors. Salt concentrations at RSL sites have not been identified from CRISM data, but anhydrous chlorides lack distinctive absorption bands (24).

To produce brine seeps from groundwater, there must be sufficient liquid to fill the pore space between particles and create a hydraulic gradient to initiate and maintain water flow to the surface. Although many RSL occur in favorable topographic locations for groundwater (Fig. 2 and figs. S3 and S4), some do not (Fig. 1). Another difficulty is that the RSL-bearing slopes are too warm to preserve shallow ground ice in equilibrium with the atmosphere (25). RSL formation, if driven by groundwater seeps, must be a nonequilibrium process, requiring ground-

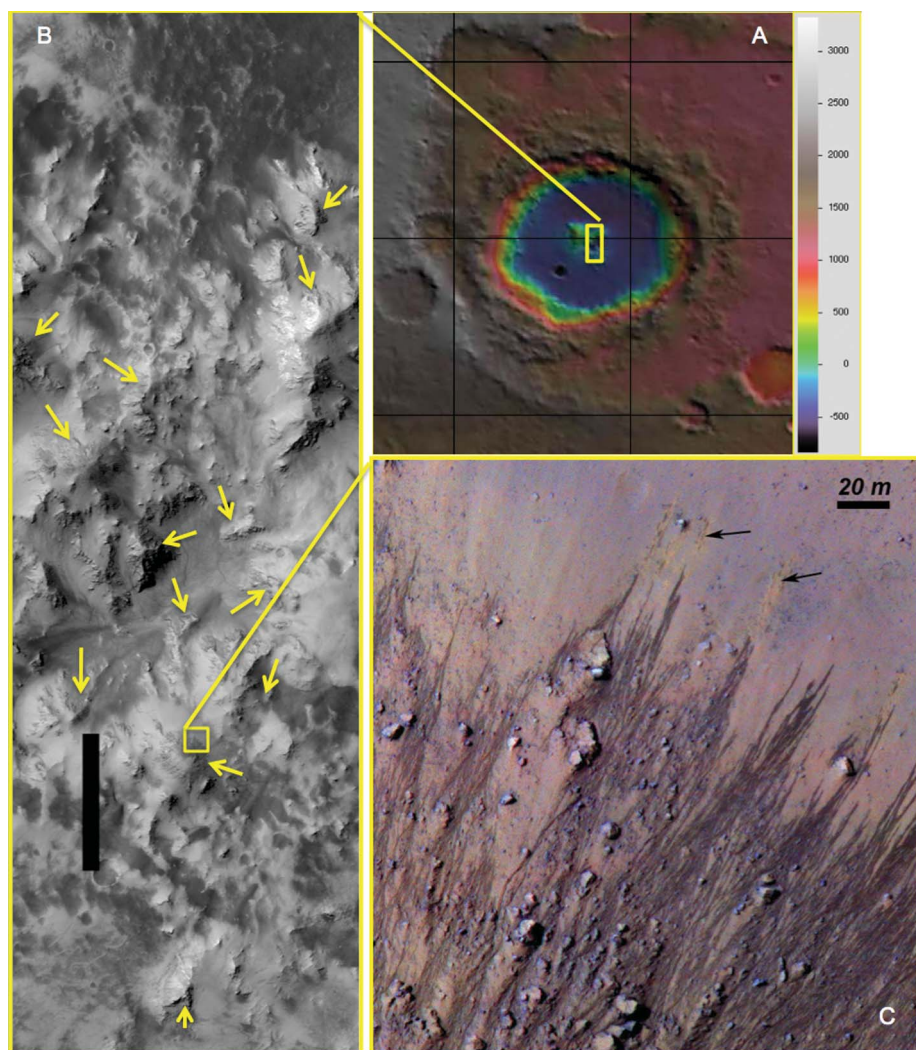


Fig. 1. RSL on the central structure of Horowitz Crater (32°S, 140.8°E), MRO Primary Science Phase (PSP) image PSP_005787_1475 ($L_S = 334$: late summer). Altimetry map (A) locates the full 5.1-km-wide HiRISE image (B), with the white box indicating the color enlargement (C). Yellow arrows in (B) show some concentrations of RSL within the central peaks and pits. Colors in (C) have been strongly enhanced to show the subtle differences, including light orange streaks (black arrows) in the upper right that may mark faded RSL. North is up on all images in this paper except fig. S4.

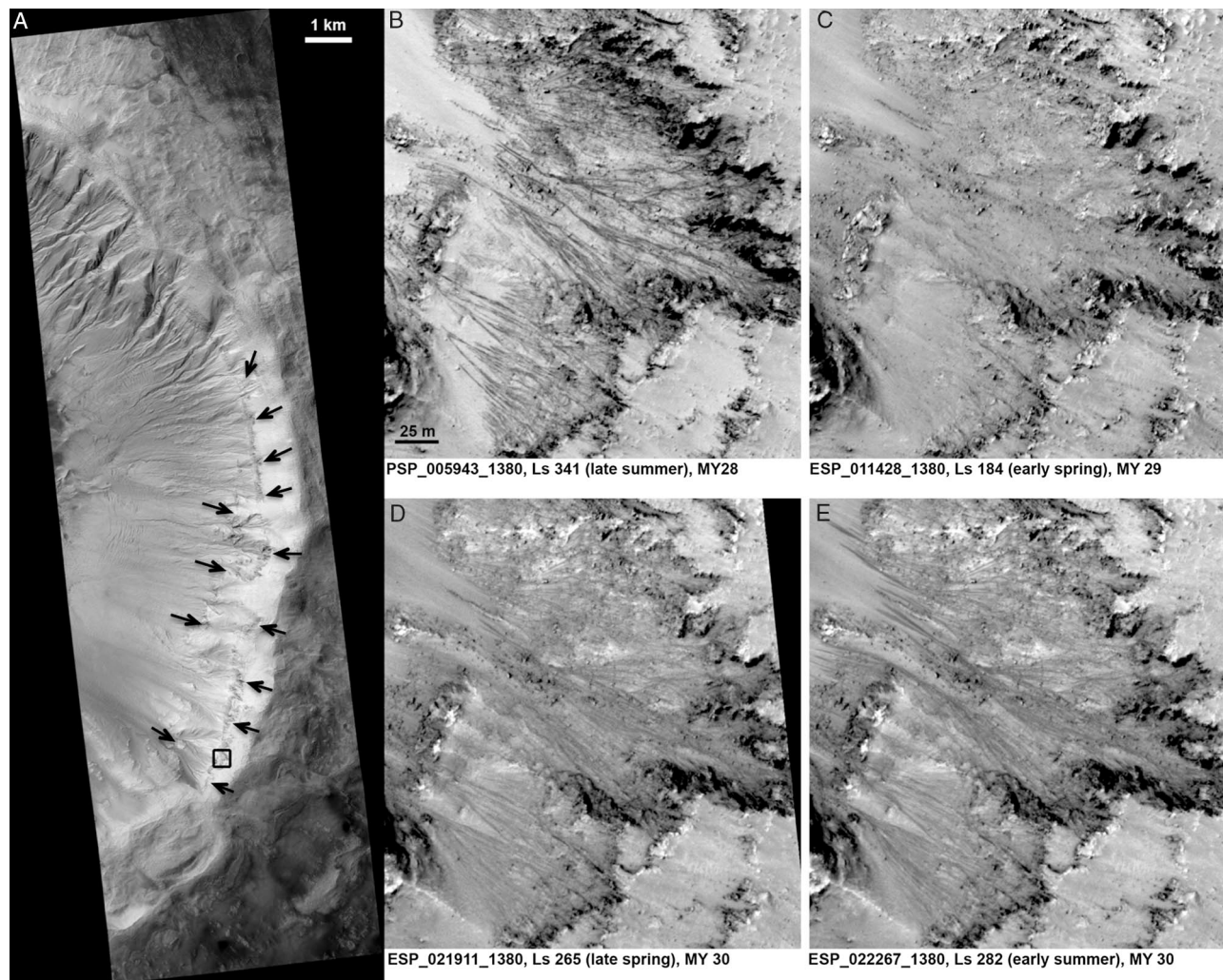


Fig. 2. Impact crater with abundant RSL at 41.6°S, 202.3°E in Newton Basin. **(A)** is the full HiRISE PSP_005943_1380; arrows point to some concentrations of RSL, and the black box locates the four blowups of orthorectified images (*13*) showing RSL (dark lines) in the late summer of MY 28 (*12*) **(B)**, faded by the next very early spring **(C)**, then grad-

ually darkening and reforming in the spring **(D)** and summer **(E)** of MY 30. The RSL are located on steep north-to-west-facing slopes associated with bedrock outcrops, often in alcoves. Each image was given a minimum-maximum stretch so that shadows are black and the brightest spots are white.

water migration or active surface processes to expose subsurface brines. Modeling by (26) shows that groundwater discharge on Martian slopes in the present-day environment requires either (i) high permeability and ample (pure) water, (ii) geothermally heated water, or (iii) brines with a depressed freezing point. The presence of brines is the most realistic scenario for Mars, requiring modest quantities of water and no geothermal heat. Furthermore, the brine model exhibits a dependence of discharge on season and favors equator-facing slopes in the middle to high latitudes (26), much like the RSL.

The mechanisms of darkening and fading of RSL are uncertain. Wetting of particulate materials causes optical darkening by a combination of processes (27), and drying or freezing would explain the fading in cold seasons, but this model is inconsistent with the lack of water absorption bands in CRISM data. Alternatively, the RSL could darken by an increase in grain size

or roughness from seeping or flows, but the fading in cold seasons still needs an explanation. The gradual settling of atmospheric dust is not a likely mechanism for the fading, based on the longer fading time scale (years, not months) of other relatively dark transient features such as slope streaks and new impact markings. Also, removal of dust during RSL formation would cause a strong color change that is not observed (SOM). RSL surface structure might change in cold seasons by a mechanism not currently understood.

We have not found any candidate RSL in the northern mid-latitudes. This may be explained by the current seasonal asymmetry, by differences in bedrock geology, or both. The putative chloride deposits, hypothesized to result from the ponding of surface runoff or groundwater upwelling, are strongly concentrated in low-albedo regions of the southern hemisphere (24), similar to the distribution of RSL. Brines forming the chloride

deposits might infiltrate or remain underground and could be stable over geologic time in the middle latitudes in a liquid or frozen state, until new craters or troughs expose the brines on warm slopes. This could explain the association of RSL with bedrock layers, either because they control the subsurface migration of fluids or water vapor or because they contain hygroscopic salt-rich lenses such as buried chloride deposits.

Liquid water on Mars today would be of great interest for astrobiology. Its presence has been suggested previously. Water flow is one hypothesis for the formation of the active mid-latitude gullies (28), although recent observations show that gullies are active in the winter and in places where seasonal CO₂ is present and water is least likely (29, 30). Briny flows have been suggested (17) for high-latitude dune streaks that appear during CO₂ defrosting, but CO₂ is the more likely driving volatile (18). Brines have been suggested for slope streaks (22), but there is no

Table 2. Slope streaks versus RSL.

Attribute	Slope streaks	RSL
Slope albedo	High (>0.25)	Low (<0.2)
Contrast	~10% darker	Up to 40% darker
Dust index*	High ($e < 0.95$)	Low ($e > 0.96$)
Thermal inertia	Low (<100)	180 to 340
Width	Up to 200 m	Up to 5 m
Slope aspect preferences	Varies with regional wind flow (15)	Equator-facing in middle latitudes
Latitudes; longitudes	Corresponds to dust distribution	32°S to 48°S; all longitudes
Formation L_5	All seasons (31)	$L_5 = 240$ to 20
Fading time scale	Years to decades	Months
Associated with rocks	No	Yes
Associated with channels	No	Yes
Abundance on a slope	Up to tens	Up to thousands
Regional mineralogy	Mars dust	Variable
Formation events	One event per streak or streaks	Incremental growth of each feature
Yearly recurrence	No	Yes

*1350 to 1400 cm^{-1} emissivity (e) (SOM).

seasonality to their formation (31). The Phoenix lander may have observed droplets of brine on the lander legs (9), and perchlorates should form liquids at times (8, 32), but definitive evidence for liquid at the landing site is lacking (33).

References and Notes

1. B. C. Clark, *Icarus* **34**, 645 (1978).
2. G. W. Brass, *Icarus* **42**, 20 (1980).
3. S. W. Squyres *et al.*, *Science* **306**, 1709 (2004).
4. A. Gendrin *et al.*, *Science* **307**, 1587 (2005).
5. M. H. Hecht *et al.*, *Science* **325**, 64 (2009).

6. D. W. G. Sears, J. D. Chittenden, *Geophys. Res. Lett.* **32**, L23203 (2005).
7. T. Altheide, V. Chevrier, C. Nicholson, J. Denson, *Earth Planet. Sci. Lett.* **282**, 69 (2009).
8. M.-P. Zorzano, E. Mateo-Marti, O. Prieto-Ballesteros, S. Osuna, N. Renno, *Geophys. Res. Lett.* **36**, L20201 (2009).
9. N. O. Rennó *et al.*, *J. Geophys. Res.* **114**, E00E03 (2009).
10. D. Möhlmann, K. Thomsen, *Icarus* **212**, 123 (2011).
11. A. S. McEwen *et al.*, *Icarus* **205**, 2 (2010).
12. L_5 is the true anomaly of Mars in its orbit around the Sun, measured from the vernal equinox, used as a measure of the season on Mars. $L_5 = 0$ corresponds to the beginning of northern spring; $L_5 = 180$ is the

beginning of southern spring. The numbering of Mars years (MYs) was defined to facilitate comparison of data sets across decades and multiple Mars missions; year 1 started on 11 April 1955.

13. Time sequences in animated GIF format are posted at <http://hirise.lpl.arizona.edu/sim/>. These are stacked cutouts from orthorectified HiRISE images archived (or to be archived within 1 year) in the Planetary Data System.
14. S. L. Murchie *et al.*, *J. Geophys. Res.* **112**, E05S03 (2007).
15. J. J. Wray, S. L. Murchie, S. W. Squyres, F. P. Seelos, L. L. Tornabene, *Geology* **37**, 1043 (2009).
16. D. Baratoux *et al.*, *Icarus* **183**, 30 (2006).
17. A. Kereszturi *et al.*, *Icarus* **207**, 149 (2010).
18. C. J. Hansen *et al.*, *Science* **331**, 575 (2011).
19. P. R. Christensen *et al.*, *Space Sci. Rev.* **110**, 85 (2004).
20. H. Viles *et al.*, *Geophys. Res. Lett.* **37**, L18201 (2010).
21. R. Ulrich, T. Kral, V. Chevrier, R. Pilgrim, L. Roe, *Astrobiology* **10**, 643 (2010).
22. M. Kreslavsky, J. W. Head, *Icarus* **201**, 517 (2009).
23. K. J. Kossacki, W. J. Markiewicz, *Icarus* **210**, 83 (2010).
24. M. M. Osterloo, F. S. Anderson, V. E. Hamilton, B. M. Hynek, *J. Geophys. Res.* **115**, E10012 (2010).
25. M. T. Mellon, W. C. Feldman, T. H. Prettyman, *Icarus* **169**, 324 (2004).
26. J. M. Goldspiel, S. W. Squyres, *Icarus* **211**, 238 (2011).
27. H. Zhang, K. J. Voss, *Appl. Opt.* **45**, 8753 (2006).
28. M. C. Malin, K. S. Edgett, L. V. Posiolova, S. M. McColley, E. Z. Dobra, *Science* **314**, 1573 (2006).
29. C. M. Dundas, A. S. McEwen, S. Diniega, S. Byrne, S. Martinez-Alonso, *Geophys. Res. Lett.* **37**, L07202 (2010).
30. S. Diniega, S. Byrne, N. T. Bridges, C. M. Dundas, A. S. McEwen, *Geology* **38**, 1047 (2010).
31. C. M. King, N. Schorghofer, K. L. Wagstaff, *Lunar Planet. Sci. Conf.* **41**, 1542 (2010).
32. S. C. Cull *et al.*, *Geophys. Res. Lett.* **37**, L22203 (2010).
33. C. R. Stoker *et al.*, *J. Geophys. Res.* **115**, E00E20 (2010).

Acknowledgments: This research was supported by NASA's MRO project; we thank them along with the reviewers. All original data reported in this paper are tabulated in the SOM and archived by NASA's Planetary Data System.

Supporting Online Material

www.sciencemag.org/cgi/content/full/333/6043/740/DC1
SOM Text
Figs. S1 to S6
Tables S1 to S5
References (34–48)

25 February 2011; accepted 17 June 2011
10.1126/science.1204816

Reduced Interannual Rainfall Variability in East Africa During the Last Ice Age

Christian Wolff,^{1,2,3} Gerald H. Haug,^{3,4*} Axel Timmermann,⁵ Jaap S. Sinninghe Damsté,^{6,7} Achim Brauer,¹ Daniel M. Sigman,⁸ Mark A. Cane,⁹ Dirk Verschuren¹⁰

Interannual rainfall variations in equatorial East Africa are tightly linked to the El Niño Southern Oscillation (ENSO), with more rain and flooding during El Niño and droughts in La Niña years, both having severe impacts on human habitation and food security. Here we report evidence from an annually laminated lake sediment record from southeastern Kenya for interannual to centennial-scale changes in ENSO-related rainfall variability during the last three millennia and for reductions in both the mean rate and the variability of rainfall in East Africa during the Last Glacial period. Climate model simulations support forward extrapolation from these lake sediment data that future warming will intensify the interannual variability of East Africa's rainfall.

In the tropics, changes in rainfall patterns have severe consequences for millions of people. East Africa, in particular, has in recent years

experienced both extreme flooding and severe droughts, with serious impacts on developing economies and wildlife throughout the region

(1). Seasonality in East African climate is controlled primarily by the biannual migration of the Intertropical Convergence Zone (ITCZ) across the region (2) (fig. S1). As a result, equatorial East Africa experiences two climatological rainy seasons (3). Dry seasons are windy because of the trade winds that straddle the ITCZ. Interannual variations in the seasonal migration of the East African ITCZ are driven to a large extent by the El Niño Southern Oscillation (ENSO) (4) and its related western Indian Ocean sea surface temperature (SST) anomalies (5, 6). El Niño events alter the atmospheric circulation, often generating an equatorial Indian Ocean SST pattern that is warmer in the west and cooler in the east, a configuration sometimes referred to as the positive phase of the Indian Ocean Dipole Mode (7). Surface ocean warming in the western Indian Ocean leads to intensification and shifts of the ITCZ, bringing more precipitation to East Africa and weakening the local surface winds (8, 9) (Fig. 1A). El Niño thus tends to enhance East African rainfall indirectly



Supporting Online Material for

Seasonal Flows on Warm Martian Slopes

Alfred S. McEwen,* Lujendra Ojha, Colin M. Dundas, Sarah S. Mattson, Shane Byrne,
James J. Wray, Selby C. Cull, Scott L. Murchie, Nicolas Thomas, Virginia C. Gulick

*To whom correspondence should be addressed. E-mail: mcewen@lpl.arizona.edu

Published 5 August 2011, *Science* **333**, 740 (2011)
DOI: 10.1126/science.1204816

This PDF file includes:

SOM Text
Figs. S1 to S6
Tables S1 to S5
References (34–48)

Supplementary Online Material (SOM) for:

Seasonal Flows on Warm Martian Slopes

Alfred S. McEwen^{1*}, Lujendra Ojha¹, Colin M. Dundas², Sarah S. Mattson¹, Shane Byrne¹, James J. Wray³, Selby C. Cull⁴, Scott L. Murchie⁵, Nicolas Thomas⁶, Virginia C. Gulick⁷

¹Lunar and Planetary Laboratory, University of Arizona, Tucson, AZ 85721, USA.

²U.S. Geological Survey, Flagstaff, AZ 86001, USA.

³Department of Astronomy, Cornell University, Ithaca, NY 14853, USA.

⁴Department of Earth and Planetary Sciences, Washington University, St. Louis, MO 63130, USA.

⁵Johns Hopkins University/Applied Physics Laboratory, Laurel, MD 20723, USA.

⁶Physikalisches Institut, University of Bern, Bern, Switzerland

⁷NASA Ames Research Center and SETI Institute, Moffett Field, CA 94035, USA.

In this SOM we present *(i)* Tables S1-S4 with data summaries, and identifiers (IDs) of images and spectral image cubes available from the Planetary Data System and experiment websites; *(ii)* additional figures to illustrate RSL morphology, setting, and behavior; and *(iii)* additional discussion of data analysis and interpretations.

Images examined for RSL with negative results are not listed, but the statistics are summarized in Figure S1. It is not possible to search every HiRISE image at full resolution, so we concentrated on completed stereo images and other images overlapping the stereo images, which insures at least 2 time steps to search for changes. Once it became clear that RSL were strongly concentrated in the southern hemisphere and during southern summer, additional images fitting these constraints were examined, as well as new images targeted to monitor RSL. We examined at high resolution only those sites that contain apparently steep slopes in the browse images or stereo anaglyphs, a total of 1925 images (~500 locations). We then examined only the steep slopes at full resolution to look for candidate RSL. A full list of HiRISE stereo pairs is available at http://hirise.lpl.arizona.edu/stereo_pairs.php.

RSL were first discovered using high resolution (1m/post) Digital Terrain Models (DTMs; 34). Change detection algorithms employed on a pair of orthorectified images revealed flow-like features on a late summer image that had faded in the subsequent image acquired in early spring. Following this discovery, HiRISE stereo images of steep slopes were examined in all latitudes and seasons, and a strong correlation of RSL to latitude and season was observed (Table S3). RSL are mostly seen on equator-facing slopes in the southern middle latitudes, although also common on west and east-facing slopes. There is no clear slope aspect preference for the more equatorial sites (Table S3), as might be expected as the sub-solar latitude reaches 25.1°S at the summer solstice and pole-facing slopes at lower latitudes will receive the greatest insolation for part of each year.

There is a distinct seasonality to RSL. They are present and well defined in images acquired during the warm season (late spring to early fall) and faded or absent in cold-season images. This is true for every image in Table S3 except some of those near the equator. Figure S2 plots the data with season for the seven confirmed RSL sites.

A number of observational biases could affect interpretations of the HiRISE images. Albedo features like RSL are easiest to identify at low phase angles, due to a backscattering surface and less contrast from topographic shading. Furthermore, the phase angle in the southern middle latitudes is generally lowest near summer solstice, and higher in cold seasons. However, phase angle changes by about $\pm 30^\circ$ by rolling the spacecraft up to 30° to the east or west, and large rolls ($>9^\circ$) are routinely used for stereo imaging. By comparing image sequences such as that

over Horowitz crater (13), where phase angle varies strongly within a short time period, we see no evidence that this affects our ability to detect the presence and distribution of RSL. We see systematic RSL changes with time, specifically appearance and growth in the warm seasons and fading in cold seasons, in spite of fluctuations in phase angles.

Another possible source of bias is atmospheric opacity, which tends to be highest in southern summer. The high opacity makes it more difficult to detect RSL, as can be seen in particular in images from MY28 that included a planet-encircling dust storm in southern summer. However, except when the opacity is unusually high, we see more rather than fewer RSL in the high-opacity southern summer, and they appear faded in the low-opacity seasons, the opposite relation to what's expected from this bias. (Furthermore, the dust opacity may have an important effect on RSL activity if they involve brines, as the dust warms the atmosphere.)

Illumination angle has a definite affect on our ability to confidently identify RSL, distinguishing these albedo markings from the topographic shading of small channels that they often follow. We have identified more RSL on west (sun)-facing slopes than on east-facing slopes where RSL may hide in the shadows or be difficult to distinguish from topographic shading. Although color imaging often helps distinguish topographic shading from surface units of differing brightness (and color), that isn't the case for RSL which have the same color (within measurement errors) as their background slopes. A special very-low-phase observation acquired over Horowitz crater (ESP_0022243_9050) clearly distinguishes the albedo markings at this time and place. The animated gifs (13) are especially useful to show these relations.

The distribution of HiRISE imaging over Mars (*11*) is another bias. For example, there is denser HiRISE coverage from 32°-48°S than most equatorial regions, to survey and monitor gullies. However, the stereo coverage is more globally uniform, with good sampling of steep rocky slopes and bedrock wherever found, and this initial survey of stereo images showed a strong latitudinal concentration of RSL. The high-latitude regions (>60°N and S) are well sampled by HiRISE but contain few steep slopes due to ice-related processes.

CRISM data were examined at several locations where the RSL-stripped slopes (*e.g.*, Figs 1-2) cover at least a few CRISM pixels (Table S4). We used CRISM full-resolution (~18 m/pixel) observations processed to I/F (ratio of reflected to incident spectral radiance) using the latest radiometric calibration (“version 3”) and a spatial/spectral filter to mitigate noise (*35*). These I/F data were then processed using standard procedures (*36*), including division by the cosine of the solar incidence angle to minimize photometric effects and atmospheric CO₂ removal via division by a scaled transmission spectrum derived from observations over Olympus Mons. Spectra from multiple pixels covering RSL slopes were averaged to maximize signal-to-noise ratio, and the resulting average spectra were divided by a spectral average from a dusty or otherwise spectrally “neutral” region in the same CRISM scene. This spectral ratio method suppresses residual artifacts (*35*) while accentuating spectral signatures in the numerator spectrum that are unique relative to the denominator.

We found no consistent spectral signature unique to the partially RSL-covered slopes. At one location, on a crater wall in Newton basin (FRT00016D70; Fig 2), some spectral ratios contained a 1.9 μm feature consistent with absorption by H₂O in hydrated minerals (*37*). This

possible hydration was found at locations where RSL were observed over one Mars year earlier (HiRISE PSP_005943_1380), but the CRISM data were acquired in mid/late autumn, when few RSL remained visible. Furthermore, other previous RSL locations on the same crater wall lack a hydration signature. Simultaneous CRISM and HiRISE images are planned at this site during the current southern summer.

At each of the other sites examined (Table S4), the CRISM data were acquired simultaneously with HiRISE images showing RSL. In none of these cases do the RSL regions exhibit hydration, although in Asimov crater (FRT00009216) the outcrops where many RSL originate appear hydrated. A slope with many RSL in Horowitz crater (FRT00008573; see Figure 1 of main text) may have a distinctive—but ambiguous—spectral signature. Other nearby hills in Horowitz crater exhibit diverse lithologies (mafic and secondary minerals) with no apparent relationship to the RSL concentrations.

Measurements of wet and dry Martian regolith simulant shows wet/dry reflectance ratios ranging from ~0.3 to 1.0 over a 2° to 130° phase angle range (38). The RSL/adjacent area ratio is ~0.6 following atmospheric correction at 33° phase angle (image used for Fig 1C), greater than the wet/dry ratio of ~0.35 at this phase angle with the Mars simulant. However, the RSL slopes are about half as reflective as the Mars simulant and less fractional darkening with wetting is expected for darker materials (27). There is no definite change in color ratio values, within the uncertainties, for either dry to wet Mars simulant or RSL to adjacent areas on Mars. Freezing and drying could explain the fading and disappearance of RSL; salt deposits could explain

brighter deposits in some faded RSL (Fig 1C). However, this wetting hypothesis is difficult to reconcile with the absence of hydration features in CRISM spectra.

“Water tracks” in the McMurdo dry valleys (39), zones of enhanced soil moisture that route briny water down steep slopes over the shallow ice table, might be useful terrestrial analogs for RSL. Their sizes, albedo, seasonal recurrence, and geologic settings are quite similar to RSL. However, shallow ice should be unstable under RSL-bearing slopes, and atmospheric processes on Mars are very different than in Antarctica. Furthermore, such features should produce strong water absorption bands in CRISM data even when filling less than half the area of each CRISM pixel.

In several of the time sequences (13) there are subtle large-scale bands of darkening that appear to move down slopes concurrent with RSL formation. This is best seen at the two fresh 4-km impact craters (Figs S3-S4). A series of shaded-relief images (matching illumination of each actual image) derived from the DTM for the sequence illustrated in Figure S3 shows that differences in illumination of the topography probably doesn't explain the bands of darkening. Photometric correction of the images is needed to better understand this.

A significant open question for wet RSL models is the source of H₂O. Evaporation rates (7) imply substantial water loss at RSL slope temperatures during the season in which they are visible, and would require corresponding amounts of water supplied; however, this constraint is relaxed if RSL are dark due to surface structure rather than wetness, consistent with CRISM observations. Groundwater flows could account for many of the characteristics of RSL, but some RSL occur near local topographic highs where groundwater outflow is less likely. A radar

search for shallow aquifers in the Newton crater basin found none (40), although small or irregular aquifers might have gone undetected. Deliquescent salts could gather atmospheric water, but the daytime relative humidity is extremely low. Salts could also draw water vapor from subsurface sources. Out-of-equilibrium ground ice at some depth sublimates slowly (unless very far from equilibrium, in which case it would not persist long), so a large source region would be required for each RSL. An alternative source might be seasonal release of adsorbed water. Adsorbed water concentrations at the surface can vary by several weight percent, but such variation is primarily observed at high latitude (41). Another option is melting of frozen brine near its eutectic temperature, but it may be difficult to preserve such brines near the equator, where ice is currently unstable on any slope (42). A very low water activity is required to have a major effect on the equilibrium stability regime of ground ice. In summary, although we can't explain in detail where the water might come from, there are sources of water on Mars and the RSL are rare features, so they may well be due to unusual conditions.

Table S5 summarizes the key observations about RSL and compares them to four formation models: wet debris flows, dry dust avalanches or granular flows, brine flow in the shallow subsurface, and briny surface flow. Briny flow (surface and/or subsurface) provides the best match to HiRISE observations, but the lack of water or salt features in CRISM spectra remain difficult to explain.

Future MRO and laboratory measurements are being planned to better understand and test hypotheses to explain the RSL. HiRISE will continue to observe a few key sites at greater time resolution (about every 2-6 weeks) to observe how RSL form and evolve over a Mars year.

CRISM will use a super-resolution mode on some observations to increase the down-track resolution, and will be able to compare spectra over time to better isolate the RSL contribution. For laboratory measurements, we are planning new bidirectional reflectance measurements on wet and dry Mars analog materials, expanding on previous work (38) to include measurements at the specular point, using lower-albedo Mars analog materials such as basaltic soil, measurement at Mars-like daytime temperatures, better control over possible drying during measurements, and improved blue light source calibration. Spectral reflectance measurements of brines and briny soils are also being planned.

Table S1. Data on Confirmed and Likely RSL

Table S1. Data on Confirmed and Likely RSL								
Features seen to change within a Mars year; present late spring to early fall.								
Green (confirmed) indicates those with direct evidence of recurrence in multiple warm seasons.								
Lat. (°S)	Lon. (°E)	Setting	Slope-Facing Direction	L _s limits on RSL activity	THEMIS IR ID	THEMIS image L _s	THEMIS BTR (K) [†]	Time of day [‡]
48.1	242.5	Fresh 4-km crater	N, NE	308-321 245-280	I17541004	331	265-269	16
47	5	Troughs in Asimov crater (5 different locations)	N, NE, NW	265-19	I17699007 I17075007 I18011005 I17699007 I09425003 I17100005 I34432003 I18011005	338 309 351 338 338 341 310 351	240-264 250-278 220-250 260-274 260-274 260-270 260-274 220-250	16 16 16 16 16 16 16 16
45.9	9.5	Fresh 4-km crater	N	259-290 257-278	I07977007 I17599005	298 333	267-287 240-270	16 16
43.5	35.0	Scarp in Rabe crater	N, E	323, 326	I34144002 I33308002 I16450002	327 287 278	270-284 283-296 269-282	14 15 16
43.7	34.1	Scarp in Rabe crater	N, E	252-328	I01410002 I07714003 I17698005 I25373005 I33308002 I34456002	355 258 338 307 287 341	220-240 259-270 233-251 247-253 260-285 246-254	15 17 16 16 15 15
42.3	201.8	Crater in Newton basin	N	259-338	I00830002 I01192002 I17817007 I33689002	330 346 343 305	254-280 230-265 240-258 281-297	15 15 16 14
41.6	202.3	Fresh crater in Newton basin	N	341, 247-282	I00830002 I01192002 I33689002 I34263004	330 346 305 332	263-280 259-265 287-297 266-276	15 15 14 14
40.3	319.7	Gullied impact crater	NW	250-285	I08553004 I16540003	300 282	278-281 275-280	16 16
39.4	202.7	Crater in Newton basin	NW, W	259-326	I00830002 I33689002 I34263004 I34575002	330 305 332 346	279-280 280-297 260-278 266-276	15 14 14 14
39	223.7	Fresh crater	N, W	340	Not Available			
38.8	159.5	Impact crater	N, W	354 252-263	I26367005	352	242-252	16
38.1	224	Fresh crater	N	310	I16431002	277	264-287	16
38.1	188.8	Graben	N	10.5, 299	I33178002 I09506004 I17181002	280 344 314	288-293 245-255 269-274	16 16 16
37.4	229	Fresh 7.5-km crater	NW	340	I07932003 I09567004 I34025002	269 347 321	276-285 253-257 286-289	17 16 14
37.1	192	Impact crater	N	330-8 272	I08520003 I16507004 I34201002	299 330 281	260-287 260-280 251-267	16 14.6 16.5
34.1	134.5	Fresh 6.6-km crater	NW	343	I17133004	312	255-280	16

32	140.8	Horowitz crater central structure	N, E, W, S	300-334 254-288	I07623002 I16384002 I17919002	253 274 347	255-275 256-276 230-260	17 16.6 16.1
14.6	175.5	MER Spirit location	NA	NA	I34027002 I16932002 I06798002	322 302 210	249-293 250-295 210-265	14.6 16 17

Notes:

* A range of L_s values (e.g., 308-340) indicates that RSL activity occurred between these times within a Mars year, whereas a single L_s value means that fresh-looking RSL, assumed to be active or very recently active, are present in just a single image per year at that time, and faded or absent in others.

† THEMIS brightness temperature at 9 microns assuming emissivity 1 and atmospheric opacity 0 (19). Lower emissivity and higher atmospheric opacity would both raise the estimated surface temperature (43). Data extracted from 100-m scale pixels over RSL-covered slopes.

‡ Time of day with 24 “hours” or increments in the Mars day (or sol). Note that THEMIS usually observes in the middle to late afternoon, after the likely peak temperature of the day for these thermal inertias (hours 13-14).

§ Blank rows are to keep Microsoft Word from eating text in the bottom row of a page.

Table S2. Starting and ending slopes of RSL, from HiRISE 1 m/pixel Digital Terrain Models.

Stereo images and RSL sites	Source slope (°)	End slope (°)	Lat. (°S)	Lon. (°E)
PSP_006261_1410 & ESP_014093_1410				
Site 1	35.1	27.9	39.18	159.44
Site 2	35.1	29.5	39.17	159.44
Site 3	33.5	31.0	39.18	159.45
Site 4	31.6	29.8	39.17	159.46
Site 5	32.8	29.8	39.17	159.47
Site 6	34.5	29.9	39.17	159.47
Site 7	34.5	30.6	39.17	159.47
PSP_005913_1640 & PSP_005201_1640				
Site 1	34.6	30.6	16.07	296.27
Site 2	32.8	31.9	16.04	296.28
PSP_005943_1380 & ESP_011428_1380				
Site 1	34.3	28.1	41.99	202.29
Site 2	32.7	30.3	41.98	202.29
Site 3	33.9	29.7	41.98	202.28
Site 4	38.1	29.4	41.97	202.29

Table S3. Data on properties of regions around confirmed and likely RSL (shaded green) and

candidate RSL (no shading).

Table S3. Data on properties of regions around confirmed and likely RSL (shaded green) and candidate RSL (no shading).

Candidates are features matching the morphology and geologic setting of RSL but without changes observed.

Lat	Lon (°E)	Image IDs	MY	Ls	Phase Angle (°)	Elev. (km)*	TES albedo†	TI‡	Dust cover§	% H ₂ O	Notes
-52.3	157.7	ESP_014146_1275	29	314	45.2	0.3	0.159	252	0.975	3.729	No other image to see changes
-49.4	14.6	PSP_005673_1305 PSP_005739_1305	28 28	329 332	51.4 41.7	0.6	0.152	252	0.972	2.956	Lineae same in both images—not RSL or no longer active by L _s 329 at this location.
-48.6	223.7	ESP_022174_1310	30	277	37.0	2.1	0.156	280	0.975	3.402	Fresh 1-km crater, NW-facing slopes, good RSL morphology but no other images
-48.5	129.7	ESP_014358_1310	29	324	43.6	1.6	0.184	180	0.965	4.63	No other image to see changes
-48.1	242.5	ESP_014011_1315 ESP_014288_1315 ESP_020947_1315 ESP_021514_1315 ESP_021870_1315 ESP_022226_1315 ESP_022437_1315	29 29 30 30 30 30 30	308 321 217 245 263 280 290	43.4 32.9 57.1 45.8 44.3 48.1 42.4	1.8	0.144	237	0.976	2.869	Fresh crater (see figure), RSL growth from L _s 308-324; faded (gone) by L _s 217, new growth L _s 245-290 (so far).
-47.6	4.6	PSP_006003_1320 PSP_006715_1320 PSP_006926_1320 ESP_016156_1320	28 29 29 29	343 11 19 34	56.2 67.0 64.2 66.7	-0.7	0.145	328	0.969	2.858	Asimov crater. RSL growth L _s 343-11 and 11-19; fading by 16156 (next Mars year)
-47.5	5.5	ESP_013334_1320 ESP_013967_1320	29 29	276 306	43.6 29.8	-1.4	0.147	340	0.969	2.881	Asimov crater. Incremental growth L _s 276-306; not very common here
-47.1	4.2	ESP_013110_1325 ESP_013611_1325	29 29	265 290	23.2 33.7	0.5	0.148	211	0.97	2.858	Asimov crater. Incremental growth L _s 265-290
-46.9	4.2	PSP_002812_1330 ESP_014178_1330	28 29	194 316	55.2 35.0	0.4	0.149	220	0.97	2.858	Asimov crater. RSL in 14178, not present the previous year in 2812
-46.9	5.1	ESP_013189_1330 ESP_013835_1330	29 29	269 300	37.4 58.6	0.1	0.139	267	0.967	2.881	Asimov crater. Incremental growth and new RSL, L _s 269-300
-45.9	9.5	ESP_012991_1335 ESP_013624_1335 ESP_021628_1335 ESP_021773_1335 ESP_022195_1335	29 29 30 30 30	259 290 251 258 278	48.2 29.4	1.5	0.16	224	0.973	2.881	Growth L _s 259 to 290, or last years' remnants in 12991 and new RSL in 13624; new RSL L _s 258-278 (latest Mars year)
-45.7	248	ESP_013457_1340	29	282	35.3	2.0	0.143	289	0.985	2.729	No other image to see changes
-43.7	34.1	PSP_004024_1360 PSP_005646_1360 ESP_021693_1360	28 28 30	252 328 254	44.3 29.2 44.6	-0.5	0.109	290	0.972	3.053	In Rabe crater. New RSL from L _s 252 to 328. Faded or gone in 21693_1360. Nice examples of emanation from specific bedrock layers.
-43.5	35	PSP_005514_1360 ESP_014401_1360	28 29	323 326	43.3 40.3	-0.8	0.152	310	0.976	3.053	In Rabe crater. RSL in both images from separate summers, different exact locations but same general regions
-43.2	145.3	ESP_014331_1365	29	323	40.3	1.5	0.18	199	0.96	3.909	No other image to see changes

-43.2	343.2	PSP_006162_1365 PSP_007085_1365	28 29	350 25	51.0 59.4	-1.1	0.167	245	0.966	3.141	RSL in central hills; active before L _s 350; didn't fade by L _s 25
-42.3	201.8	PSP_003675_1375 PSP_004163_1375 PSP_005877_1375	28 28 28	235 259 338	49.9 18.8 66.1	0.2	0.144	275	0.971	3.298	RSL abundant in 5877; not apparent in 4163 (but hazier). Maybe faded RSL in 3675. Crater with many lava layers of even thickness.
-42.2	202.0	PSP_006866_1375 PSP_007657_1375 ESP_015964_1375	29 29 30	17 45 27	58 79 81	-0.4	0.137	262	0.97	3.298	Small patches of lineae near N rim of crater in 6866; faded in 7657 and 15964. Groundwater flow challenging here.
-41.6	202.3	PSP_005943_1380 ESP_011428_1380 ESP_016808_1380 ESP_021555_1380 ESP_021911_1380 ESP_022267_1380	28 29 30 30 30 30	341 184 57 247 265 282	48.8 55.5 77.5 40.1 39.0 42.7	-0.2	0.119	200	0.972	3.298	Crater wall in Newton basin; dense RSL in 5943; faded by 11428 and in 16808. New activity L _s 247-282. Sapping morphologies.
-40.3	319.7	ESP_012795_1395 ESP_013507_1395	29 29	250 285	48.7 54.4	-1.6	0.162	282	0.969	2.078	Many RSL on NW-facing crater wall in 13507; 12795 hazy but RSL appear absent in places or very faded
-39.6	88.1	PSP_005934_1400	28	340	45.5	-4.9	0.172	259	0.958	3.18	Hazy; Hellas floor; high dust index. No other images here
-39.4	202.7	PSP_004176_1405 PSP_005587_1405	28 28	259 326	51.0 31.1	-0.6	0.125	244	0.974	3.203	RSL formed between L _s 259 to 326
-39	23.7	PSP_005929_1405 ESP_016438_1405	28 30	340 44	51.0 67.3	0.8	0.159	342	0.97	3.746	A few RSL in 5929; faded by 16438
-38.8	159.5	PSP_006261_1410 ESP_011390_1410 ESP_014093_1410 ESP_021662_1410 ESP_021873_1410 ESP_022440_1410	28 29 29 30 30 30	354 183 312 252 263 290	49.6 52.5 62.1 45.9 40.9 33.5	0.5	0.142	297	0.971	3.271	Many on N-facing slope of crater in 6261 and 14093, but different precise locations (and separate Mars years). Faded in 11390. New activity 21662-22440, so recurrence in 3 Mars years.
-38.1	224	ESP_014038_1415, ESP_016583_1415 ESP_022253_1415 ESP_022464_1415	29 30 30 30	310 49 288 291	36.1 74.4 14 36	0.4	0.144	212	0.973	2.995	Streak w bright border; RSL in small overlap region faded by L _s 49, still faded by L _s 288-291 of MY30, so recurrence not confirmed
-38.1	188.8	PSP_002370_1415 PSP_006695_1415 ESP_013736_1415 ESP_013947_1415 ESP_021595_1415	28 29 29 29 30	174 10 296 305 249	66.8 62.1 38.8 31.3 46	-0.1	0.13	217	0.965	2.944	On N-facing slope of graben. RSL in 6695 not present in 2370; changed or grown in 13736. 13947 same as 13736. 21596 same as 13736 but faded or just topo shading. Difficult to distinguish albedo from topo shading.
-37.4	229	PSP_003252_1425 PSP_005942_1425	28 28	214 340	59.2 48.6	2.3	0.153	192	0.975	2.931	More distinct RSL in 5942, different than 3252 but still faint
-37.1	192	PSP_003583_1425 PSP_005706_1425 PSP_006629_1425 ESP_013248_1425	28 28 29 29	230 331 8 272	58.9 42.5 51.8 39.8	0.0	0.132	206	0.971	2.801	No RSL in 3583, all over N slope in 5706 and 6629; initial activity between L _s 230-331; small continuation L _s 331-8; again L _s 272 next year but different part of crater wall imaged (recurrence not yet verified)

-35.7	129.4	PSP_005550_1440 PSP_009901_1440 ESP_014081_1440 ESP_014147_1440	28 29 29 29	324 123 311 314	52.7 78.5 37.5 22.1	0.0	0.153	274	0.972	3.973	Gasa crater—only a few candidates—topographic shading?
-34.1	134.5	PSP_005985_1455 ESP_013817_1455	28 29	299 343	43.7 59.6	2.0	0.13	226	0.973	3.469	A few small RSL in rocky patch, SE portion of crater, in 5985 but faded in 13817. Recurrence not observed.
-32.7	120.1	PSP_005524_1470	28	323	39.8	0.6	0.132	260	0.97	3.477	Good RSL morphology, no other image
-32	40.8	PSP_005009_1480 PSP_005787_1475 PSP_007857_1475 ESP_020832_1475 ESP_021689_1475 ESP_022177_1475 ESP_022243_9050 ESP_022256_1475 ESP_022401_1474	28 28 29 30 30 30 30 30 30	300 334 52 212 254 278 280 281 288	34.6 32.8 64.4 40.2 51.5 14.7 2.6 46.2 57.6	0.1	0.173	296	0.97	3.035	Horowitz crater central peaks/pit—dense concentrations in 5009; growth in 5787; faded in 7857, 20832, 21689, new RSL in last 3 images. Active L _s 278-288 and 300-334; faded by L _s 52. No RSL in rim regions of Horowitz crater (several summer images).
-32	41.2	PSP_007000_1475	29	22	56.4	0.2	0.179	309	0.972	3.035	West-facing slopes of Horowitz rim; no repeat coverage
-31	9.3	ESP_013240_1485	29	272	44.4	1.2	0.131	260	0.97	4.408	Faint; no repeat coverage
-18.2	41.5	PSP_007966_1615	29	56	63.9	1.6	0.143	225	0.976	4.066	Faint; no repeat coverage, N- and NW-facing slopes
-15.9	296.2	PSP_005201_1640 PSP_005913_1640 ESP_021591_1640 ESP_022158_1640	28 29 30 30	308 340 249 277	38.6 56.6 32.7 27.1	2.43	0.154	315	0.976	2.848	Isolated RSL; growth from L _s 308-340; no new activity L _s 277 of following year
-12.9	293.5	ESP_020879_1670	30	214	57.7	1.9	0.135	361	0.971	3.403	Landslide scarp; no repeat coverage
-10.5	24.6	PSP_005145_1690 PSP_005567_1690	28 28	306 325	39.9 21.4	1.8	0.125	161	0.972	5.676	New candidate RSL from L _s 305-325. Are bright streaks in 5649 faded RSL?
-8.8	304.9	PSP_005649_1710 ESP_012479_1710 ESP_021551_1710 ESP_021828_1710 ESP_021973_1710	28 29 30 30 30	328 234 247 260 268	31.7 34.5 68.7 31.8 47.5	0.8	0.128	264	0.976	3.451	S side of Elorza crater central pit; TSL in 5649 faded in later images. Many very small lineae, perhaps many more below HiRISE resolution.
-6.8	298.0	ESP_013033_1730 ESP_013745_1730 ESP_019336_1730 ESP_019969_1730 ESP_021815_1730	29 29 30 30 30	262 296 146 173 260	47.9 53.5 64.6 49.5 50.5	-1.0	0.174	343	0.975	3.585	Pits in Hydræ Chasma, only a few streaks and minor changes, appears faded at L _s 146, then redarkens (?) and some grow a little at L _s 262 and 296. Not typical RSL, but equatorial seasons different.
+10.0	157.8	PSP_003650_1900 PSP_004283_1900 PSP_008924_1900	28 28 29	234 265 88	55.3 30.0 49.6	-2.4	0.246	323	0.956	4.248	Cerberus Fossae. A few new lineae from L _s 233 to 265; one of which appears gone by 88.5. High dust index and color contrast unlike confirmed RSL.
+18.5	65.0	PSP_001385_1985 ESP_022074_1985	28 30	134 273	42.8 54.8	-0.3	0.119	277	0.972	3.252	Fresh crater in Baldet crater, a few RSL-like features at L _s 134 (late northern summer); faded in much later (2.5 Mars years) image.

Notes:

* Elevation from Mars Orbiter Laser Altimeter (44)

† Albedo from Thermal Emission Spectrometer (45)

‡ Nighttime Thermal Inertia in $\text{Jm}^{-2}\text{s}^{-1/2}\text{K}^{-1}$ (46)

§ Dust Cover index is 1350-1400 cm^{-1} emissivity (47)

|| Percent H_2O as inferred from the Gamma Ray Spectrometer (GRS) (48)

¶ Data in columns with noted above are 5x5 pixel medians to avoid noisy pixels. Individual pixels cover larger areas than the RSL-covered slopes. GRS data is especially low resolution (>100 km).

⁷ Blank rows are to keep Microsoft Word from eating text in bottom row of page.

Table S4. CRISM observations analyzed at locations of known RSL.

Latitude (°S)	Longitude (°E)	L_s	CRISM image	Simultaneous HiRISE
47.74	4.58	11	FRT00009216	PSP_006715_1320
43.24	343.27	25	FRT00009B5D	PSP_007085_1365
41.55	157.73	57	FRT00016D70	ESP_016808_1380
32.05	140.82	334	FRT00008573	PSP_005787_1475
32.04	140.80	281	FRT00002E7C	ESP_022243_9050

Table S5. RSL Suitability Matrix: Model (top) vs. Observation (left). Y (green) indicates consistency between observation and model; N (red) indicates lack of consistency.

Model:	Wet debris flow	Dry dust avalanche or grain flow	Brine flow in shallow subsurface	Briny surface flow
Observation:				
Follow steep downhill gradient	Y	Y	Y	Y
Darken surface	Y (rougher surface texture)	Y (removing dust, depositing dark grains, or rougher surface)	Y (wetting or changing surface texture)	Y (wetting or changing surface texture)
No strong color contrast with background slopes	N (in places with diverse colors of bedrock and colluvium)	N (removing dust should make RSL less red; depositing grains should change color in places with diverse colors of colluvium)	Y	Y
Formation and growth when surface temperature 250°-300° C	Y (brine in liquid state)	?? (sublimate ice to make grains less sticky)	Y (brine in liquid state)	Y (brine in liquid state)
Known source of sufficient water	N	Y (no water needed)	N	N
Fading (and sometimes brightening) in cold seasons	? (dust deposition too slow; unknown mechanism to change surface texture)	? (dust deposition too slow and they fade during the least-dusty season; some unknown mechanism to change surface texture less likely with no volatile)	? (Yes if initial darkening due to wetting—problematic from CRISM data, or unknown mechanism to change surface texture). Brightening could be from residual deposits of salt or fine-grained materials.	? (Yes if initial darkening due to wetting—problematic from CRISM data, or unknown mechanism to change surface texture). Brightening could be from residual deposits of salt or fine-grained materials.
Lack of water bands in CRISM	Y (most of surface dry when observed)	Y	Y (surface stays mostly dry; darkening not by wetting)	? (surface quickly dries out after each flow advance; darkening not from wetting)
Lack of strong spectral signature of salts in CRISM	Y	Y	Y	? (Yes if liquid consistently infiltrates before significant evaporation, or salts lack IR absorption bands).
Episodic, incremental growth	? (incremental growth not typical, but maybe nighttime freezing of water stops motion)	N (once initiated, flow should continue until stability reached, and would not remain on the brink of stability for future incremental flows.)	Y (activity varies with diurnal temperature and atmospheric conditions)	Y (activity varies with diurnal temperature and atmospheric conditions)
Lack of resolved topography	N (difficult—even if each flow is too thin to see, they should build up over many years, and new RSL should be diverted around old deposits)	N (difficult—topographic changes detected from dust avalanches)	Y	Y (bulk of flowing material infiltrates or evaporates/sublimates)
Concentrated in Latitude 32-48 S	Y (latitude controls water availability)	N	Y (latitude controls water availability)	Y (latitude controls water availability)
10³ – 10⁴ lineae within a HiRISE image	? (not typical of debris flows)	N	Y (if water source is widespread)	Y (if water source is widespread)
Associated with rocky slopes	Y	? (unless initiated by rock falls?)	Y (bedrock controls water availability)	Y (bedrock controls water availability)
Yearly recurrence at same locations	N (should remove loose debris and make future flows less likely at these same locations)	N (should remove loose debris and make future flows less likely at these same locations)	Y (if water available in same places)	Y (if water available in same places)
Flow around obstacles like boulders; no uphill or	N (unless deposits are too thin even after multiple years)	N (unless deposits are too thin even after multiple years)	Y	Y

downhill deposits.

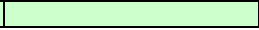
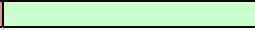


Figure S1. Locations with steep slopes examined for RSL, and the number containing confirmed or likely RSL, plotted as a function of L_s . A larger number of locations imaged in southern summer (L_s 270-360) were examined once it was clear that this was when RSL are usually present.

Figure S2. For the seven confirmed RSL sites, images with and without distinct RSL are plotted as a function of season (L_s). All images acquired from L_s 260 to 10 show distinct RSL; all images acquired from L_s 40 to 240 do not show distinct RSL.

Figure S3. RSL on a fresh 4-km diameter impact crater at 48.11°S, 242.45°E. Location maps in A and B (from ESP_014011_1315) with black boxes showing zoomed-in areas. C-H is a full-resolution (0.25 m/pixel) sequence of 6 orthorectified sub-images over the northwest-facing inner slope. RSL (dark northwest-tending lines) extend a bit between L_s 308 and 321 (mid-summer) of MY 29, fade (completely vanish) by L_s 217 (early spring) of MY 30, start to reappear by L_s 245 and grow to L_s 280 (early summer) of MY30. The new RSL follow almost, but not exactly, the same path as RSL from the previous year, following the topographic gradient. An animated gif of a larger subscene is available at <http://hirise.lpl.arizona.edu/sim/>.

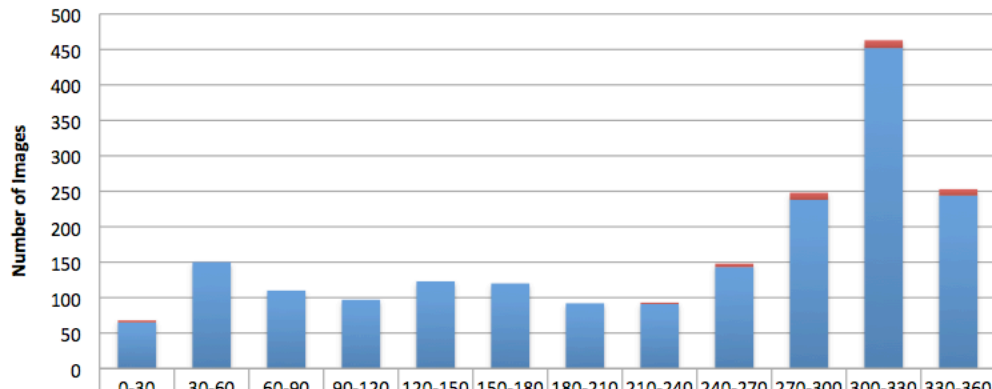
Figure S4. Color image of RSL located on the northwest-facing wall of a well-preserved 4-km impact crater at 48.1°S, 242.4°E. Black arrows point out some of the RSL, seen to grow incrementally in 3 prior images this MY and season. Although there are diverse color units in

the bedrock and colluvium, the RSL show little color contrast, appearing relatively red over relatively red surfaces, etc. ESP_022437_1315; enhanced color; north is approximately down.

Figure S5. Small area of Horowitz crater central structure, showing RSL in late summer of MY28 (top) and development of RSL in late spring-early summer of MY30 (3 bottom views). From top to bottom: PSP_005787_1475, ESP_021689_1475, ESP_022177_1475, ESP_022256_1475

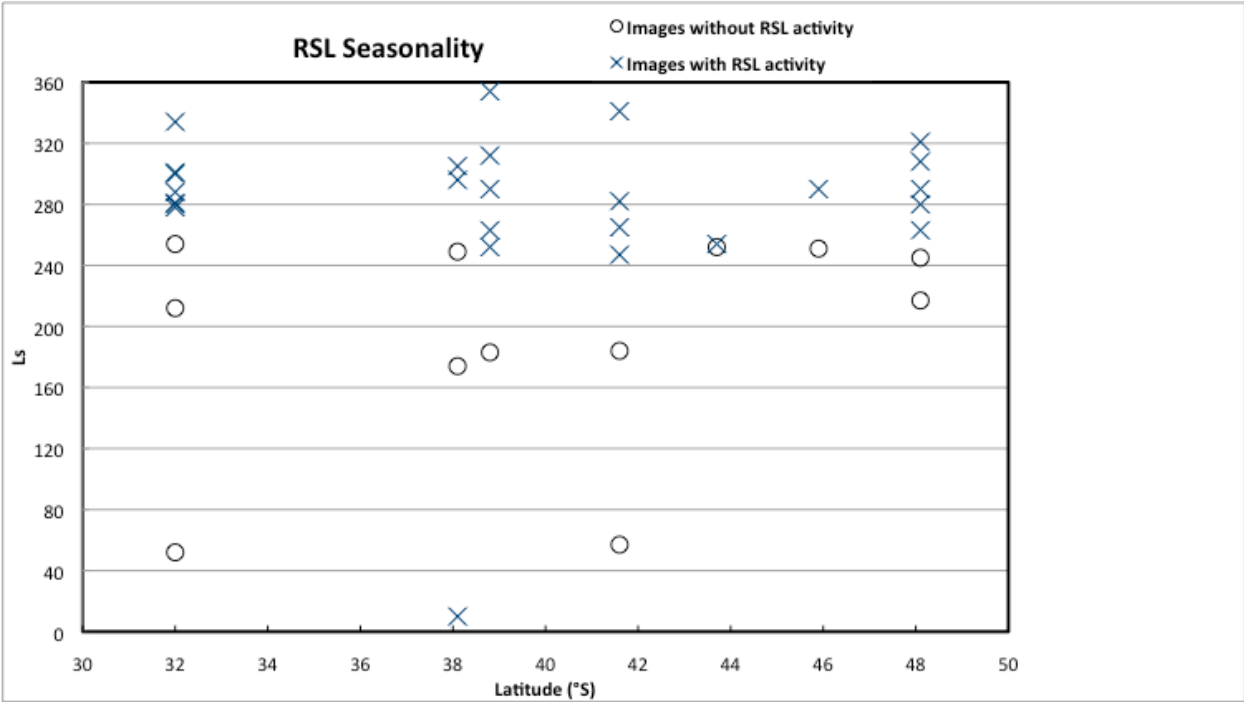
Figure S6. The puzzling nature of equatorial candidate RSL are illustrated here, in a portion of Hydræ Chasm at 6.8° S, 298.0° E. All subimages given linear stretches saturating brightest and darkest 0.1% of the pixels; images have not been orthorectified. There appears to be minor growth of dark linear features from L_s 261-296 (MY29), fading by L_s 147 (MY30), then some new growth by L_s 173 and again at 260. The first and last image of this set have nearly identical photometric angles, so real surface surface changes have occurred. The seasonal temperatures in the tropics don't vary strongly, but surfaces are heated most near L_s 250 and least near L_s 70 from orbital eccentricity. Maybe this represents very limited RSL activity.

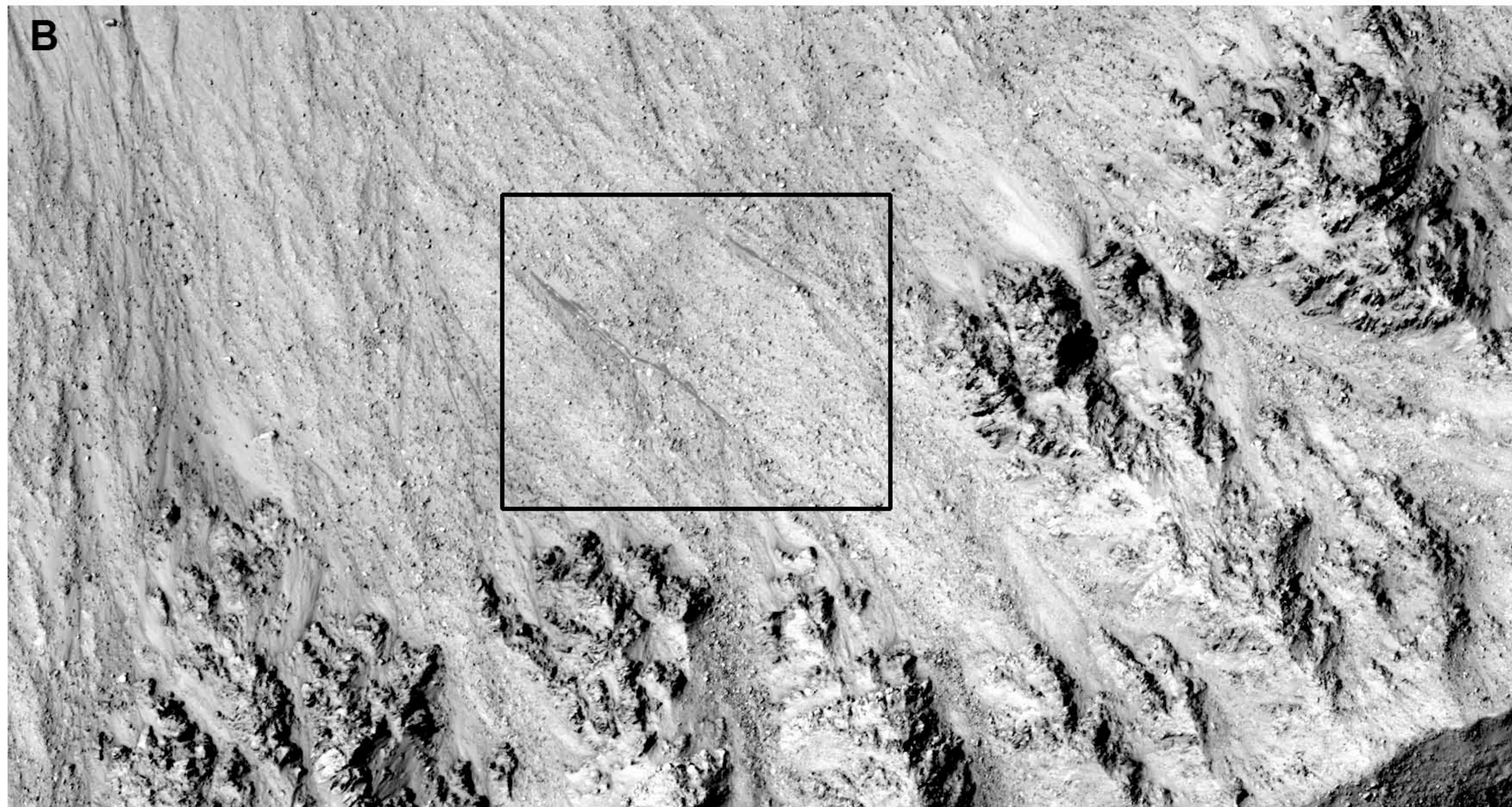
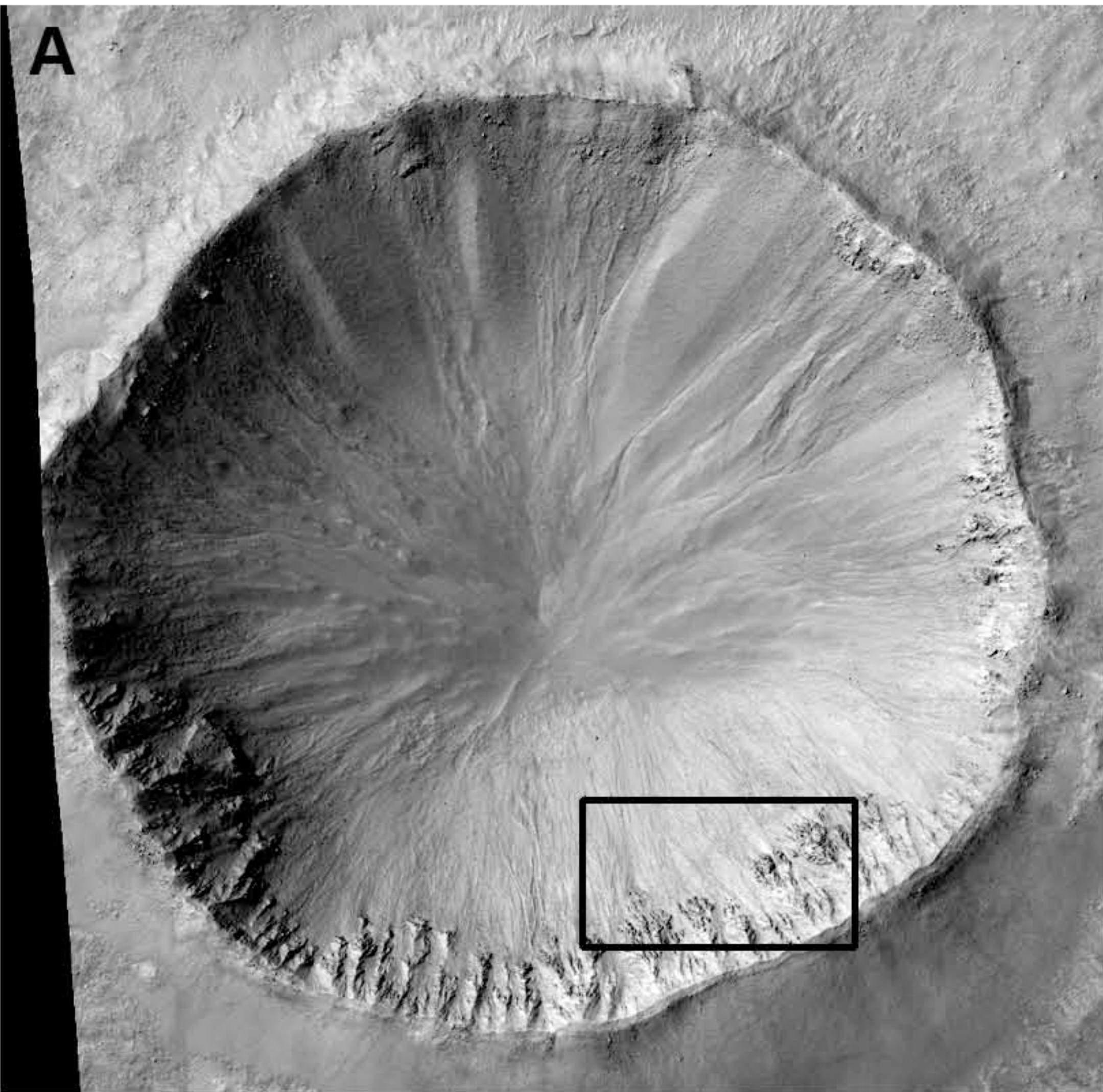
Frequency of Images with RSL vs. Season (Ls)



	0-30	30-60	60-90	90-120	120-150	150-180	180-210	210-240	240-270	270-300	300-330	330-360
Images with RSL	3							2	5	10	11	9
Total number of Images Examined	65	150	110	97	123	120	92	91	143	238	452	244

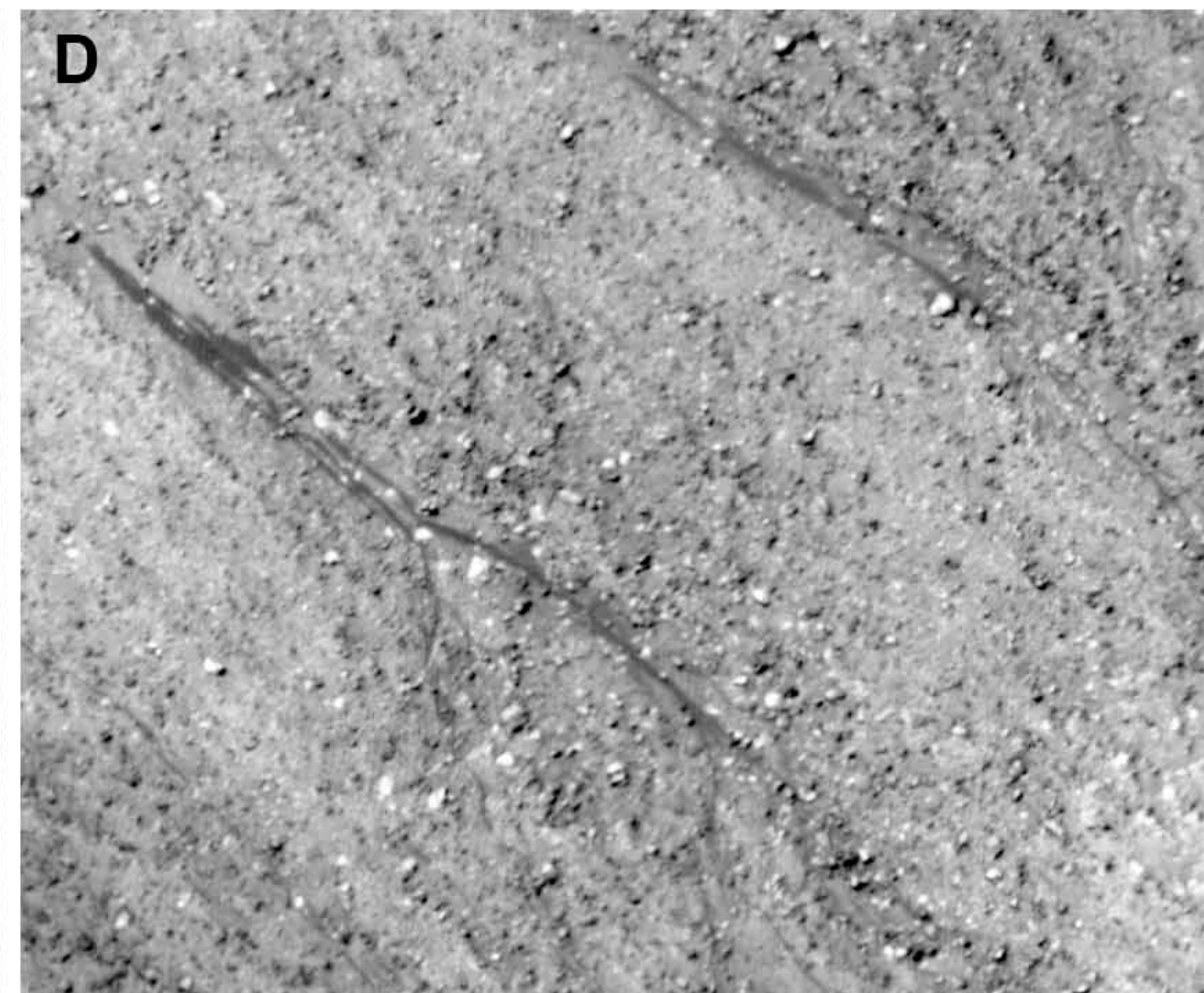
Ls





ESP_014011_1315, Ls 308 MY 29

25 m



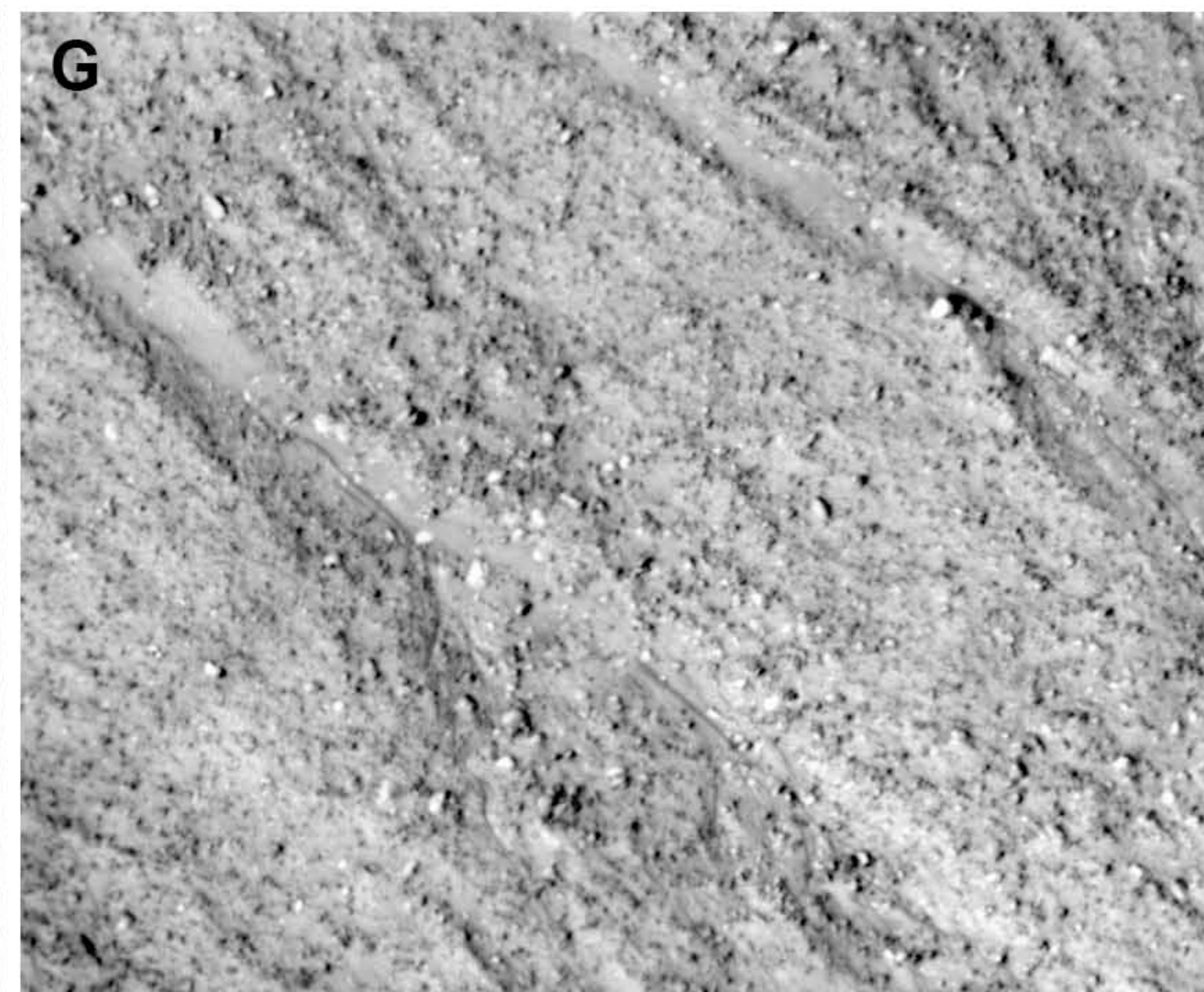
ESP_014288_1315, Ls 321, MY 29



ESP_020947_1315, Ls 217, MY 30



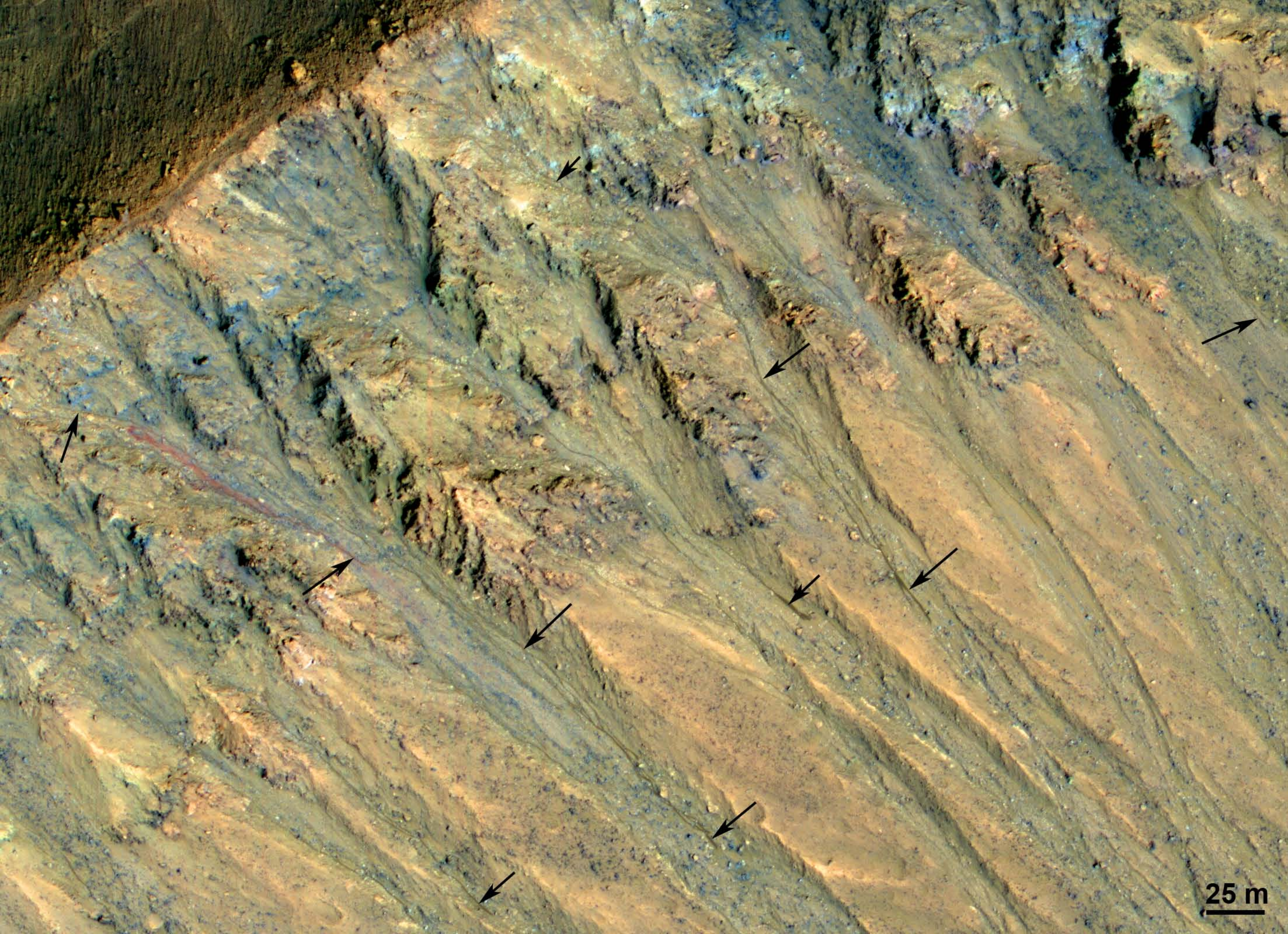
ESP_021514_1315, Ls 245, MY 30

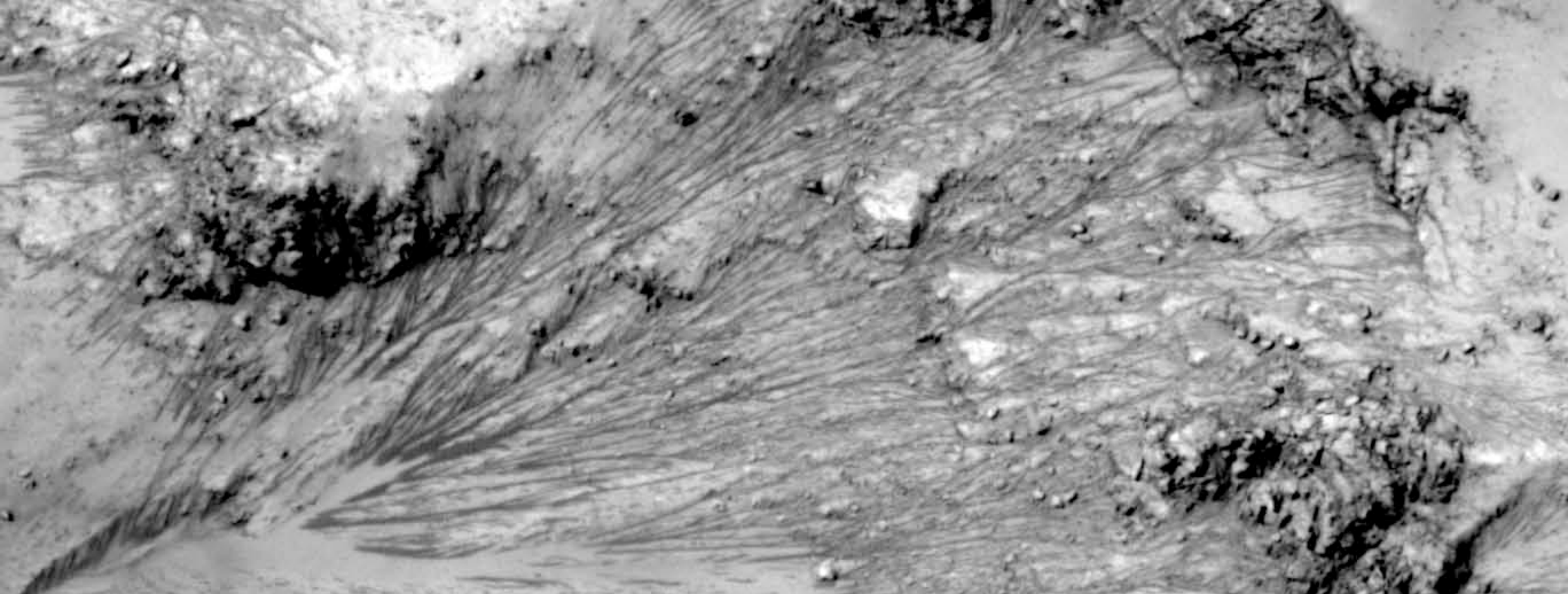


ESP_021870_1315, Ls 263, MY 30

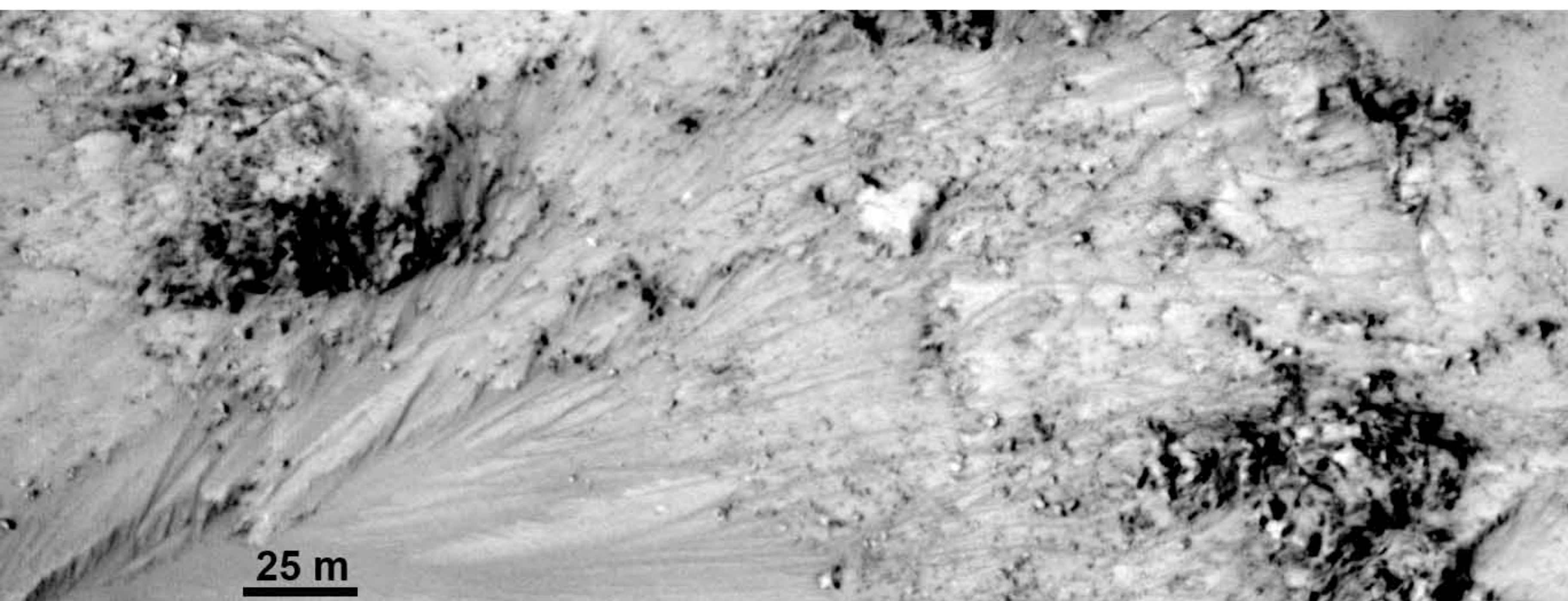


ESP_022226_1315, Ls 280, MY 30

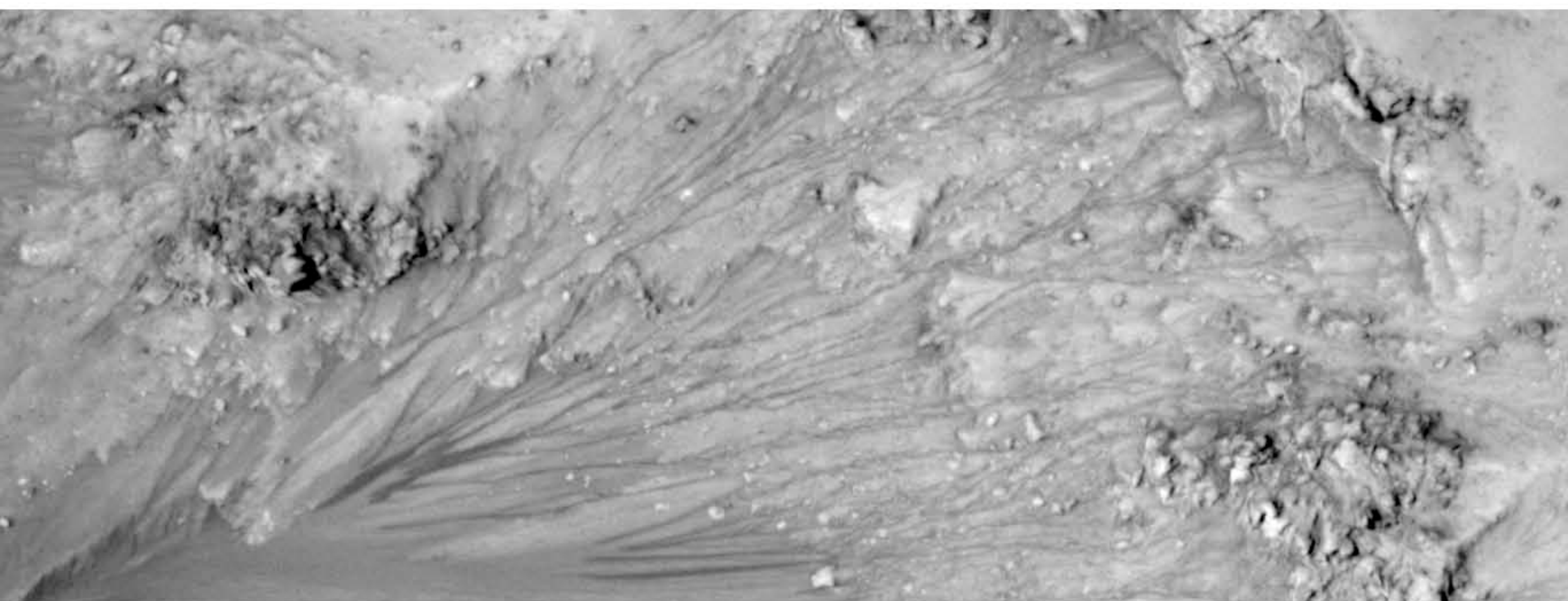




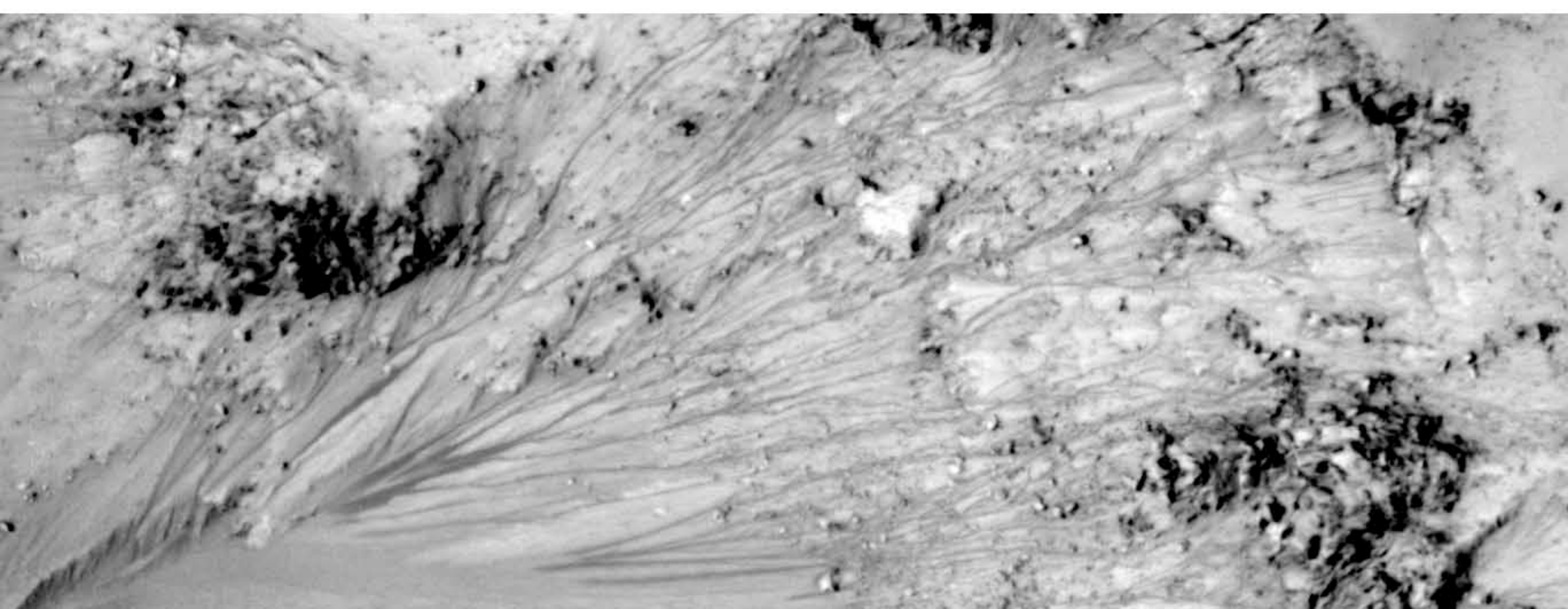
**MY28
Ls 334**



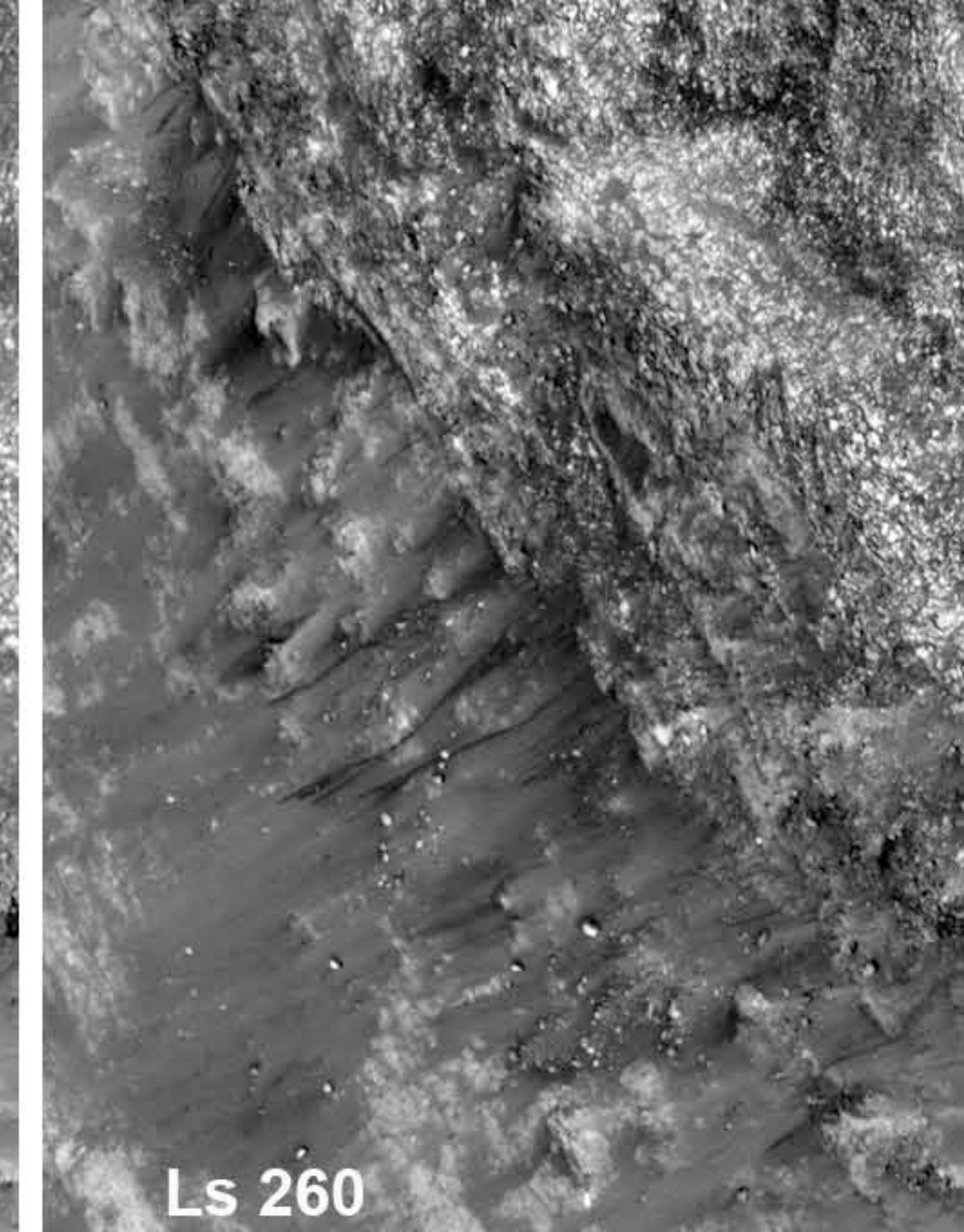
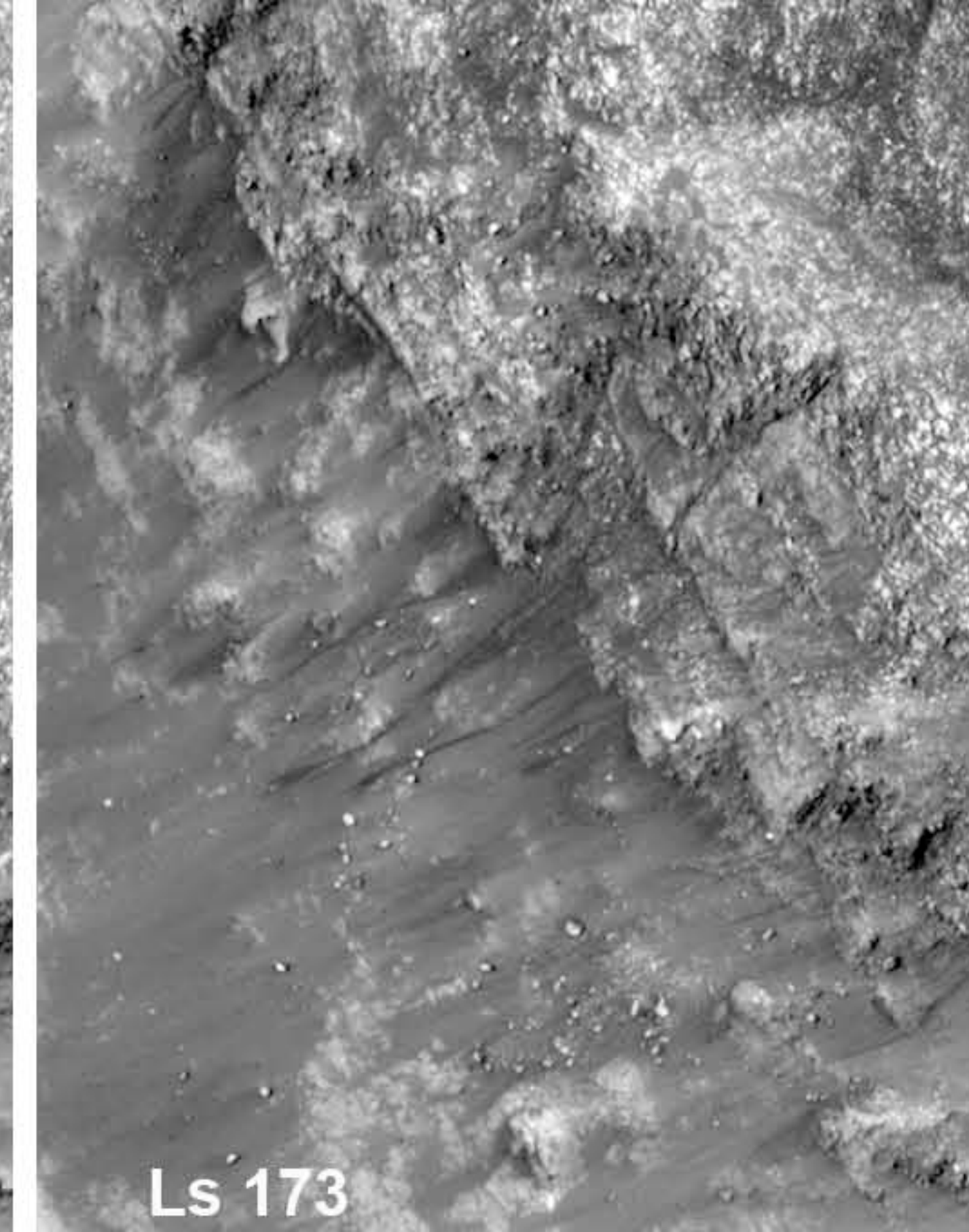
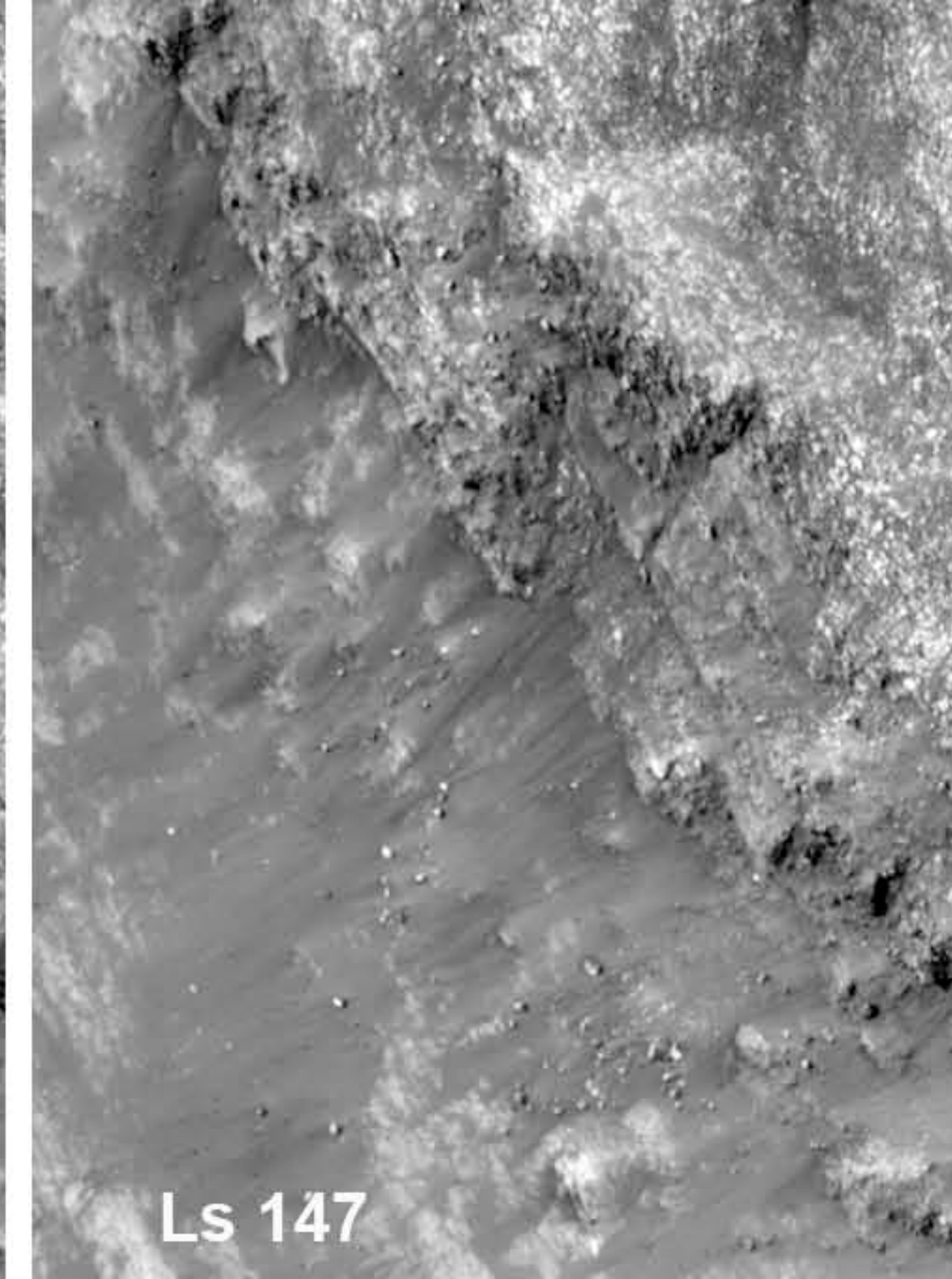
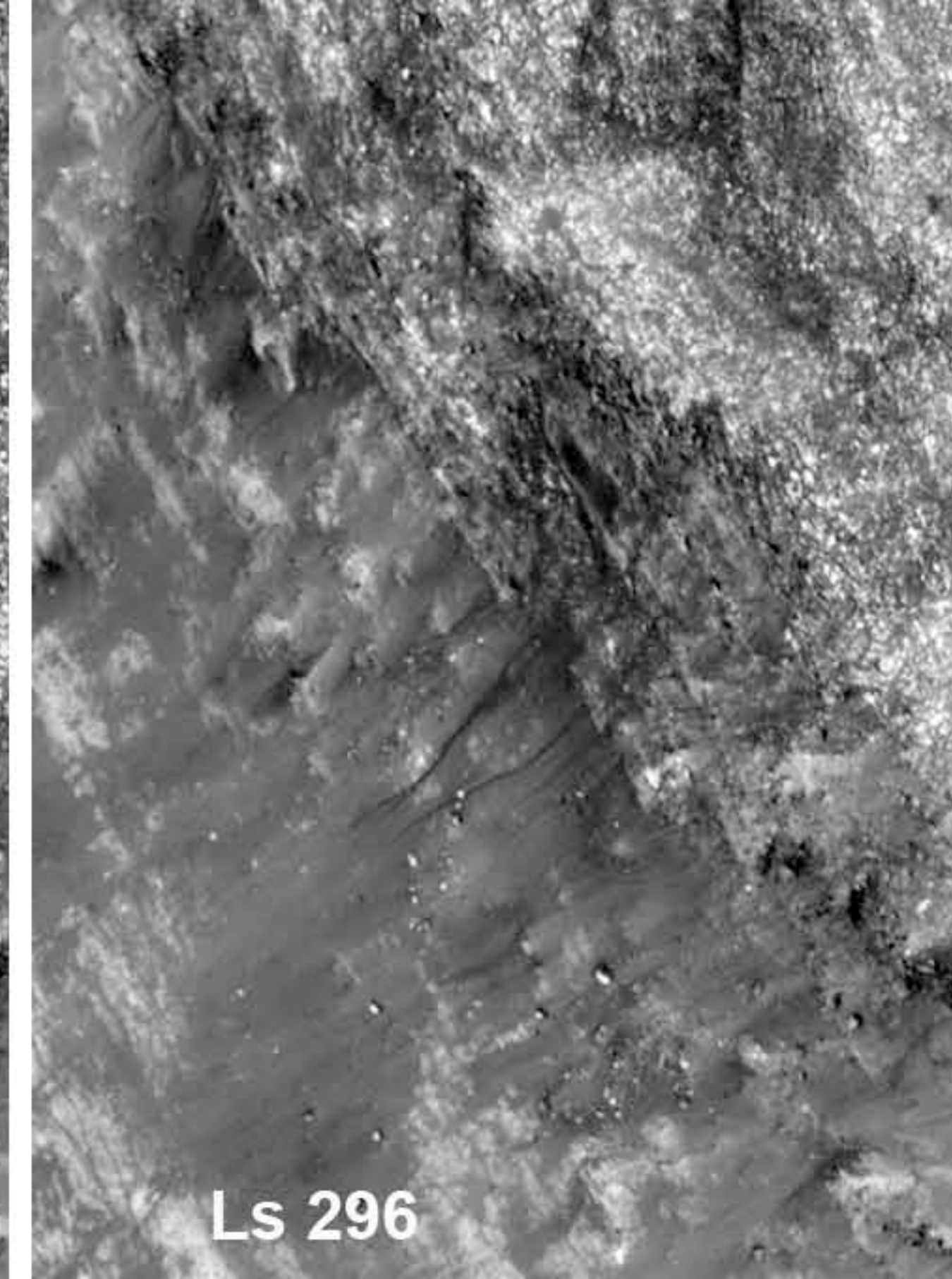
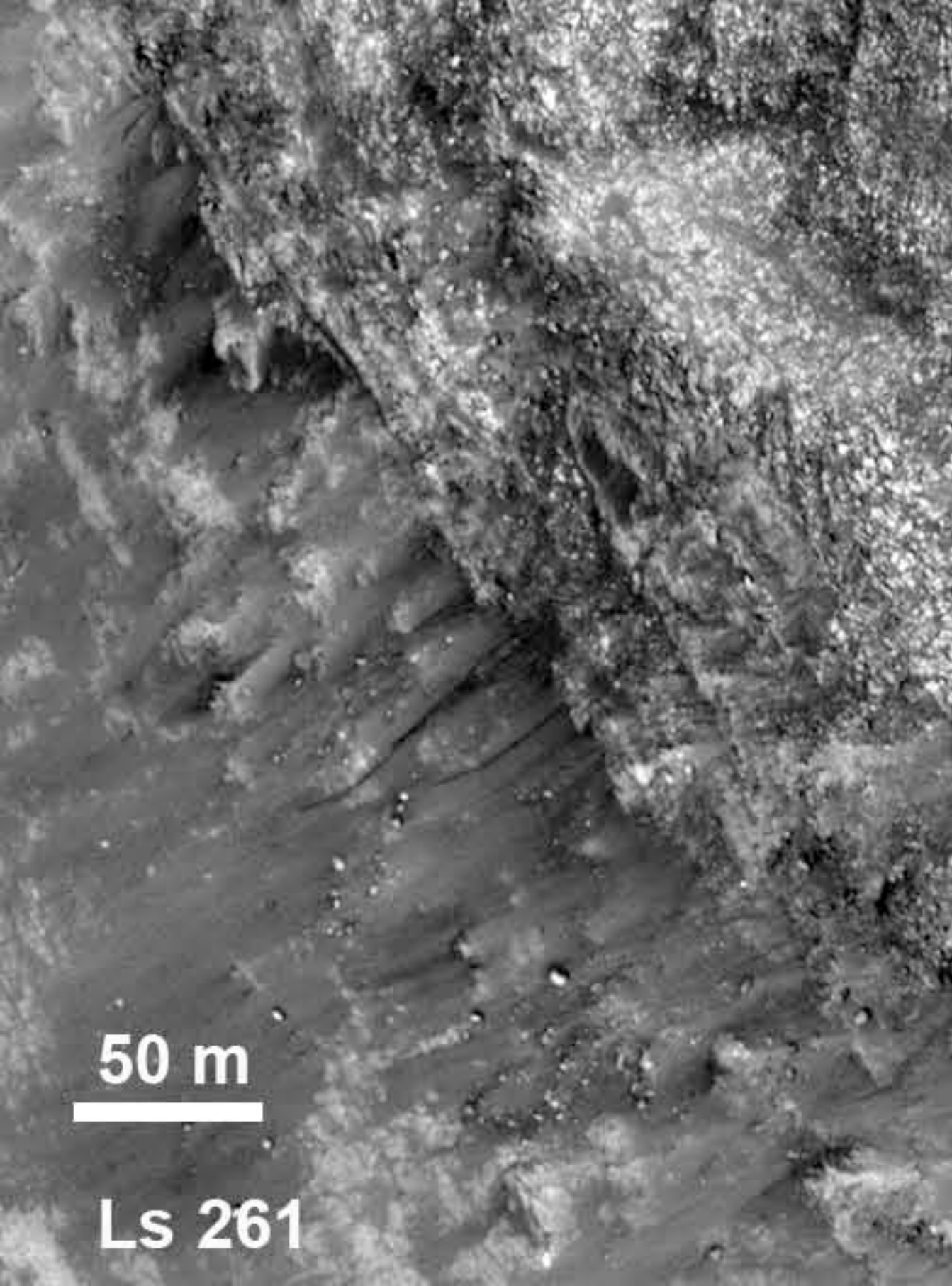
**MY30
Ls 254**



**MY30
Ls 278**



**MY30
Ls 281**



References and Notes

1. B. C. Clark, Implications of abundant hygroscopic minerals in the Martian regolith. *Icarus* **34**, 645 (1978). [doi:10.1016/0019-1035\(78\)90052-0](https://doi.org/10.1016/0019-1035(78)90052-0)
2. G. W. Brass, Stability of brines on Mars. *Icarus* **42**, 20 (1980). [doi:10.1016/0019-1035\(80\)90237-7](https://doi.org/10.1016/0019-1035(80)90237-7)
3. S. W. Squyres *et al.*, In situ evidence for an ancient aqueous environment at Meridiani Planum, Mars. *Science* **306**, 1709 (2004). [doi:10.1126/science.1104559](https://doi.org/10.1126/science.1104559) [Medline](#)
4. A. Gendrin *et al.*, Sulfates in Martian layered terrains: The OMEGA/Mars Express view. *Science* **307**, 1587 (2005). [doi:10.1126/science.1109087](https://doi.org/10.1126/science.1109087) [Medline](#)
5. M. H. Hecht *et al.*, Detection of perchlorate and the soluble chemistry of martian soil at the Phoenix lander site. *Science* **325**, 64 (2009). [Medline](#)
6. D. W. G. Sears, J. D. Chittenden, On laboratory simulation and the temperature dependence of the evaporation rate of brines on Mars. *Geophys. Res. Lett.* **32**, L23203 (2005). [doi:10.1029/2005GL024154](https://doi.org/10.1029/2005GL024154)
7. T. Altheide, V. Chevrier, C. Nicholson, J. Denson, Experimental investigation of the stability and evaporation of sulfate and chloride brines on Mars. *Earth Planet. Sci. Lett.* **282**, 69 (2009). [doi:10.1016/j.epsl.2009.03.002](https://doi.org/10.1016/j.epsl.2009.03.002)
8. M.-P. Zorzano, E. Mateo-Marti, O. Prieto-Ballesteros, S. Osuna, N. Renno, Stability of liquid saline water on present day Mars. *Geophys. Res. Lett.* **36**, L20201 (2009). [doi:10.1029/2009GL040315](https://doi.org/10.1029/2009GL040315)
9. N. O. Rennó *et al.*, Possible physical and thermodynamic evidence for liquid water at the Phoenix landing site. *J. Geophys. Res.* **114**, E00E03 (2009). [doi:10.1029/2009JE003362](https://doi.org/10.1029/2009JE003362)
10. D. Möhlmann, K. Thomsen, Properties of cryobrines on Mars. *Icarus* **212**, 123 (2011). [doi:10.1016/j.icarus.2010.11.025](https://doi.org/10.1016/j.icarus.2010.11.025)
11. A. S. McEwen *et al.*, The High Resolution Imaging Science Experiment (HiRISE) during MRO's Primary Science Phase (PSP). *Icarus* **205**, 2 (2010). [doi:10.1016/j.icarus.2009.04.023](https://doi.org/10.1016/j.icarus.2009.04.023)
12. L_S is the true anomaly of Mars in its orbit around the Sun, measured from the vernal equinox, used as a measure of the season on Mars. $L_S = 0$ corresponds to the beginning of northern spring; $L_S = 180$ is the beginning of southern spring. The numbering of Mars years (MYs) was defined to facilitate comparison of data sets across decades and multiple Mars missions; year 1 started on 11 April 1955.
13. Time sequences in animated GIF format are posted at <http://hirise.lpl.arizona.edu/sim/>. These are stacked cutouts from orthorectified HiRISE images archived (or to be archived within 1 year) in the Planetary Data System .
14. S. L. Murchie *et al.*, Compact Reconnaissance Imaging Spectrometer for Mars (CRISM) on Mars Reconnaissance Orbiter (MRO). *J. Geophys. Res.* **112**, E05S03 (2007). [doi:10.1029/2006JE002682](https://doi.org/10.1029/2006JE002682)

15. J. J. Wray, S. L. Murchie, S. W. Squyres, F. P. Seelos, L. L. Tornabene, Diverse aqueous environments on ancient Mars revealed in the southern highlands. *Geology* **37**, 1043 (2009). [doi:10.1130/G30331A.1](https://doi.org/10.1130/G30331A.1)
16. D. Baratoux *et al.*, The role of wind-transported dust in slope streak activity: Evidence from the HRSC data. *Icarus* **183**, 30 (2006). [doi:10.1016/j.icarus.2006.01.023](https://doi.org/10.1016/j.icarus.2006.01.023)
17. A. Kereszturi *et al.*, Indications of brine related local seepage phenomena on the northern hemisphere of Mars. *Icarus* **207**, 149 (2010). [doi:10.1016/j.icarus.2009.10.012](https://doi.org/10.1016/j.icarus.2009.10.012)
18. C. J. Hansen *et al.*, Seasonal erosion and restoration of Mars' northern polar dunes. *Science* **331**, 575 (2011). [doi:10.1126/science.1197636](https://doi.org/10.1126/science.1197636) [Medline](#)
19. P. R. Christensen *et al.*, The Thermal Emission Imaging System (THEMIS) for the Mars, 2001 Odyssey Mission. *Space Sci. Rev.* **110**, 85 (2004). [doi:10.1023/B:SPAC.0000021008.16305.94](https://doi.org/10.1023/B:SPAC.0000021008.16305.94)
20. H. Viles *et al.*, Simulating weathering of basalt on Mars and Earth by thermal cycling. *Geophys. Res. Lett.* **37**, L18201 (2010). [doi:10.1029/2010GL043522](https://doi.org/10.1029/2010GL043522)
21. R. Ulrich, T. Kral, V. Chevrier, R. Pilgrim, L. Roe, Dynamic temperature fields under Mars landing sites and implications for supporting microbial life. *Astrobiology* **10**, 643 (2010). [doi:10.1089/ast.2010.0472](https://doi.org/10.1089/ast.2010.0472) [Medline](#)
22. M. Kreslavsky, J. W. Head, Slope streaks on Mars: A new “wet” mechanism. *Icarus* **201**, 517 (2009). [doi:10.1016/j.icarus.2009.01.026](https://doi.org/10.1016/j.icarus.2009.01.026)
23. K. J. Kossacki, W. J. Markiewicz, Interfacial liquid water on Mars and its potential role in the formation of hill and dune gullies. *Icarus* **210**, 83 (2010). [doi:10.1016/j.icarus.2010.06.029](https://doi.org/10.1016/j.icarus.2010.06.029)
24. M. M. Osterloo, F. S. Anderson, V. E. Hamilton, B. M. Hynek, Geologic context of proposed chloride-bearing materials on Mars. *J. Geophys. Res.* **115**, E10012 (2010). [doi:10.1029/2010JE003613](https://doi.org/10.1029/2010JE003613)
25. M. T. Mellon, W. C. Feldman, T. H. Prettyman, The presence and stability of ground ice in the southern hemisphere of Mars. *Icarus* **169**, 324 (2004). [doi:10.1016/j.icarus.2003.10.022](https://doi.org/10.1016/j.icarus.2003.10.022)
26. J. M. Goldspiel, S. W. Squyres, Groundwater discharge and gully formation on martian slopes. *Icarus* **211**, 238 (2011). [doi:10.1016/j.icarus.2010.10.008](https://doi.org/10.1016/j.icarus.2010.10.008)
27. H. Zhang, K. J. Voss, Bidirectional reflectance study on dry, wet, and submerged particulate layers: Effects of pore liquid refractive index and translucent particle concentrations. *Appl. Opt.* **45**, 8753 (2006). [doi:10.1364/AO.45.008753](https://doi.org/10.1364/AO.45.008753) [Medline](#)
28. M. C. Malin, K. S. Edgett, L. V. Posiolova, S. M. McColley, E. Z. Dobrea, Present-day impact cratering rate and contemporary gully activity on Mars. *Science* **314**, 1573 (2006). [doi:10.1126/science.1135156](https://doi.org/10.1126/science.1135156) [Medline](#)
29. C. M. Dundas, A. S. McEwen, S. Diniega, S. Byrne, S. Martinez-Alonso, New and recent gully activity on Mars as seen by HiRISE. *Geophys. Res. Lett.* **37**, L07202 (2010). [doi:10.1029/2009GL041351](https://doi.org/10.1029/2009GL041351)

30. S. Diniega, S. Byrne, N. T. Bridges, C. M. Dundas, A. S. McEwen, Seasonality of present-day Martian dune-gully activity. *Geology* **38**, 1047 (2010). [doi:10.1130/G31287.1](https://doi.org/10.1130/G31287.1)
31. C. M. King, N. Schorghofer, K. L. Wagstaff, Martian slopes streaks form sporadically throughout the year. *Lunar Planet. Sci. Conf.* **41**, 1542 (2010).
32. S. C. Cull *et al.*, Concentrated perchlorate at the Mars Phoenix landing site: Evidence for thin film liquid water on Mars. *Geophys. Res. Lett.* **37**, L22203 (2010). [doi:10.1029/2010GL045269](https://doi.org/10.1029/2010GL045269)
33. C. R. Stoker *et al.*, Habitability of the Phoenix landing site. *J. Geophys. Res.* **115**, E00E20 (2010). [doi:10.1029/2009JE003421](https://doi.org/10.1029/2009JE003421)
34. R. L. Kirk *et al.*, Ultrahigh resolution topographic mapping of Mars with MRO HiRISE stereo images: Meter-scale slopes of candidate Phoenix landing sites. *J. Geophys. Res.* **113**, E00A24 (2008). [doi:10.1029/2007JE003000](https://doi.org/10.1029/2007JE003000)
35. F. P. Seelos *et al.*, CRISM data processing and analysis products update—calibration, correction, and visualization. *Lunar Planet. Sci.* **42**, 1438 (2011).
36. S. L. Murchie *et al.*, Compact Reconnaissance Imaging Spectrometer for Mars investigation and data set from the Mars Reconnaissance Orbiter's primary science phase. *J. Geophys. Res.* **114**, E00D07 (2009). [doi:10.1029/2009JE003344](https://doi.org/10.1029/2009JE003344)
37. R. N. Clark, T. V. V. King, M. Klejwa, G. A. Swayze, N. Vergo, High spectral resolution reflectance spectroscopy of minerals. *J. Geophys. Res.* **95**, 12653 (1990). [doi:10.1029/JB095iB08p12653](https://doi.org/10.1029/JB095iB08p12653)
38. K. Gunderson, B. Luthi, P. Russell, N. Thomas, Visible/NIR photometric signatures of liquid water in Martian regolith simulant. *Planet. Space Sci.* **55**, 1272 (2007). [doi:10.1016/j.pss.2007.03.004](https://doi.org/10.1016/j.pss.2007.03.004)
39. J. S. Levy, A. G. Fountain, "Water tracks" in the McMurdo dry valleys, Antarctica: A permafrost-based hydrological system supporting complex biological and geochemical processes in a Mars-like environment. *Lunar Planet. Sci. Conf.* **42**, 1210 (2011).
40. D. C. Nunes *et al.*, Examination of gully sites on Mars with the shallow radar. *J. Geophys. Res.* **115**, E10004 (2010). [doi:10.1029/2009JE003509](https://doi.org/10.1029/2009JE003509)
41. R. E. Milliken *et al.*, Hydration state of the Martian subsurface as seen by Mars Express OMEGA: 2. H₂O content of the surface. *J. Geophys. Res.* **112**, E08S07 (2007). [doi:10.1029/2006JE002853](https://doi.org/10.1029/2006JE002853)
42. O. Aharonson, N. Schorghofer, Subsurface ice on Mars with rough topography. *J. Geophys. Res.* **111**, E11007 (2006). [doi:10.1029/2005JE002636](https://doi.org/10.1029/2005JE002636)
43. A. Molina, M. A. de Pablo, M. Ramos, Testing THEMIS-derived brightness temperature by MINI-TES (Spirit) data. *Lunar Planet. Sci. Conf.* **41**, 1150 (2010).
44. D. E. Smith *et al.*, The global topography of Mars and implications for surface evolution. *Science* **284**, 1495 (1999). [doi:10.1126/science.284.5419.1495](https://doi.org/10.1126/science.284.5419.1495) [Medline](#)
45. P. R. Christensen *et al.*, Mars Global Surveyor Thermal Emission Spectrometer experiment: Investigation description and surface science results. *J. Geophys. Res.* **106**, 23823 (2001). [doi:10.1029/2000JE001370](https://doi.org/10.1029/2000JE001370)

46. N. E. Putzig, M. T. Mellon, Apparent thermal inertia and the surface heterogeneity of Mars. *Icarus* **191**, 68 (2007). [doi:10.1016/j.icarus.2007.05.013](https://doi.org/10.1016/j.icarus.2007.05.013)
47. S. W. Ruff, P. R. Christensen, Bright and dark regions on Mars: Particle size and mineralogical characteristics based on Thermal Emission Spectrometer data. *J. Geophys. Res.* **107**, 5127 (2002). [doi:10.1029/2001JE001580](https://doi.org/10.1029/2001JE001580)
48. W. V. Boynton *et al.*, Distribution of hydrogen in the near surface of Mars: Evidence for subsurface ice deposits. *Science* **297**, 81 (2002). [doi:10.1126/science.1073722](https://doi.org/10.1126/science.1073722) [Medline](#)